Phase A

ADCS Report

Prepared by:

Alvaro Foletti, EPFL - SGM

Piyawat Kaewkerd, EPFL - SMT

Checked by:

Approved by:

•

EFPL
Lausanne
Switzerland

•

7/3/2006

•

Laboratoire d'Automatique

Université Neuchâtel unine Hes·so Haute Ecole Spécialisée de Suisse occidentale EPFL ÉCOLE POLYTECHNIQUE FÉDÉRALE DE LAUSANNE

RECORD OF REVISIONS

ISS/REV	Date	Modifications	Created/modified by
1/0	June 13th 2006	Issue Draft	Created by Alvaro Foletti
1/1	June 14, 2006	Added sections, cleared order	Alvaro Foletti
1 / 2	June 15, 2006	Added sections	Alvaro Foletti
1 /3	June 16, 2006	Added sections	Alvaro Foletti
1/4	June 16, 2006	Combined the attitude determination report (disturbances, sensors, EKF, sensors baseline, etc.) into this one	Piyawat Kaewkerd
1/5	June 17, 2006	Finished integrating report added final sections.	Alvaro Foletti
1/6	June 22, 2006	Updated controller sections with new results	Alvaro Foletti
1/7	June 29, 2006	Integrated feedback from various sources	Alvaro Foletti
2.0	June 29, 2006	New Issue from 1.7	Alvaro Foletti
3.0	July 3, 2006	Updated the determination part	Piyawat Kaewkerd

FOREWORD

The goal of the Swisscube project is to develop a low-cost small satellite, to be launched in 2008, capable of operating small scientific or technological payloads. The Cubesat format (10x10x10 cm and 1 kg) was chosen because of the lower launch cost of this standard format, its relative simplicity and the possibility of collaboration with other universities developing their own Cubesats. Furthermore, several universities have already launched their own Cubesat, and this experience can help in the design of the Swisscube. The scientific purpose of the mission is to observe and take measurements of the night glow phenomenon.

Several laboratories and institutes collaborate in their respective subsystems. The objective of the Automatic Control Laboratory (LA) is to provide algorithms and insight about the attitude control and determination system (ACDS), which responsibility is to make sure that the satellite has the correct attitude in space. Due to the fact that nearly every subsystem has an impact on one another, the demanded work was highly multidisciplinary.

The Phase A, which took place during the spring semester of 2006, is a feasibility study preceding more detailed design and testing. The goal of this phase is to have more precise specifications by doing some research on the limitations, trade-offs and capabilities of each subsystem.

Piyawat Kaewkerd and Alvaro Foletti are the two master's students at the EPFL who worked on the ADCS in the context of 12-credit semester projects. Piyawat Kaewkerd worked on the determination system, which encompasses the sensors and the estimation algorithms, whereas Alvaro Foletti worked on the attitude actuators, the system dynamics and the control algorithms.

Work division by student:

Alvaro Foletti Sections:	5.1, 5.5, 5.6, 5.7, 5.8, 5.9, 6.2, 7.2, 7.3.2
Piyawat Kaewkerd Sections:	5.2, 5.3, 5.4, 5.10, 5.11, 5.12, 6.1, 7.1, 7.3.1

INTRODUCTION

For the Phase A, four objectives for the ACDS development were defined by the LA:

- Choosing the actuators and sensors of the Swisscube.
- Dynamic modeling of the Swisscube.
- Determination of Swisscube's attitude.
- Optimal controller design.

The possible choices actuators and sensors were studied, and the different selections are discussed in this report. The multiple trade-off between performance, mass, power consumption and the needed computational resources, inherent to the space systems, had to be taken into account for the baseline.

In this Phase A of the project the baseline attitude actuators were chosen and dimensioned. A dynamic model was created using a Lagrangian formulation and Tait-Bryan angle attitude description; the model was used in both the determination and the control algorithms design. The control strategy adopted was a linearized optimal least-square controller it was implemented and tested. For the estimation, an extended Kalman filter was developed and the selection of sensors was modeled and tested.

Some conclusions can be done about the capabilities of the ACDS, especially about the controllability and attainable accuracy. It is possible to control the system in its nominal conditions while the estimation algorithm and the baseline sensors, composed of magnetometers and solar panels used as sun sensors, provide a satisfying accuracy during daytime. However, during eclipses, the accuracy drops by more than three times, and the addition of other sensors might be needed.

1 REFERENCES

1.1 Normative references

[N1] SwissCube Project Specifications, Noca Muriel

1.2 Informative references

Arnini, R., Faye, P., Kjeldgaard, K., Kjaer, K., Liu, Y., Villekjaer, M., *Attitude Determination System for AAUSAT-II*, Aalborg University, 2004.

Arce, Diana, Jutzeler Benjamin, Röthlisberger, Guillaume *Design of a Swisscube Structure and Configuration*, LMAF, EPFL, Lausanne June 2006.

Alminde L., *Semi-Active Attitude Control and Off-line Attitude Determination for SSETI-Express*, Aalborg University, 2004.

Bhat Sanjay P: *Controllability of Non-linear Time Varying systems: Application to Spacecraft attitude control using magnetic actuators.* IEEE transactions on Automatic control, Vol 50, No 11, November 2005.

Brown Charles D.. *Elements of spacecraft design* Reston American Institute of Aeronautics and Astronautics, Inc.,2002.(AIAA education series)

Desponts, Bastien. Systems Engineering Report, Swisscube Project, Space Center, EPFL, Lausanne June 2006.

Ciani, Manuela *Studio del Sistema di Assetto del satellite Atmocube tramite attuatori magnetici,* Facolta di Scienze Matematiche Fisiche e Naturali, Universitá degli Studi di Trieste, Italy, 2003.

Courtois et all *Cours de Technologies Spatiale : Techniques & Technologies des Véhicules Spatiaux*, Centre National d'Etudes Spatiales, Cepadues-Editions, Toulouse 1998

Frederiksen M.K. Graversen T., Vedstesen S.V. *Attitude Control System for AAU CubeSat,* Department of Control Engineering, Institude of Electronic Systems, Aalborg University. *June 6 2002.*

Gregory, Bryan Scott, *Attitude control system design for ION, The Illinois observing nanosatellite* University of Illinois at Urbana-Champaign, Urbana, Illinois 2004

James R.Wertz, *Spacecraft attitude determination and control* written by the technical staff - Attitude Systems Operation, Computer sciences Corporation Dordrecht ; Boston : Reidel, 1978

Larson W. J., Wertz, James, R., *Space mission analysis and design*, 3rd ed., Ed. Kluwer Academic Publishers, 1999.

M. Lovera, E. D. Marchi, and S. Bittani, *Periodic attitude control techniques for small satellites with magnetic actuators IEEE* Trans. Control Syst. Technol., vol. 10, no. 1, pp. 90-95, Jan. 2002.

Psiaki, M.L., Martel, F., Pal, P.K., *Three-axis attitude determination via Kalman filtering of magnetometer data*, Journal of Guidance, Control, and Dynamics, vol. 13, pp. 506-514, May-June 1990.

Sidi, Marcel J *Spacecraft Dynamic and Control – A practical engineering approach* Cambridge Aer

Splinner, Georges *Conception de Machines Principes et Applications, Vol. 2 Dynamique* Presses Polytechniques et Universitaires Romande, Lausanne 1997

Svartveit, Kristian, *Attitude Determination of the NCUBE satellite,* Department of Engineering Cybernetics, NTNU Throndheim, Norway. January 6th 2003.

Grewal, S.M., Andrews, A.P, *Kalman Filtering*, Prentice Hall, 1993.

Humphreys, T.E., *Attitude Determination for Small Satellites with Modest Pointing Constraints.*

2 TERMS, DEFINITIONS AND ABBREVIATED TERMS

2.1 Abbreviated terms

- SRF: Satellite Reference Frame $(\hat{x}_s, \hat{y}_s, \hat{z}_s)$
- ORF: Orbital Reference Frame $(\hat{x}_o, \hat{y}_o, \hat{z}_o)$
- EKF: Extended Kalman Filter
- P-Pod: Cubesat deployment mechanism.
- COG: Center of Gravity

2.2 Definitions

- (ϕ, θ, ψ): Tate – Bryant Angles, Euler angles following a 1, 2, 3 order used to define the rotation from the ORF to the SRF.
- φ: Position of the inertial wheel with respect to the SRF, in the case of more than one wheel an index i=1, 2 or 3 is added.
- I_{ij} with i, j = x, y, z : Moments of Inertia of the Swisscube with respect to the SRF calculated at the Swisscube center of gravity, these however do not take into account the inertial wheels(s).
- (I_{wpi}, I_{wsi}) with i = 1 , 2, 3 : Polar and Side moments of inertia of the inertial wheel(s) calculated at the inertial wheel center of gravity.
- (P_{cs}, P_{wi}) with i = 1, 2, 3 : Position of the Cubesat and the inertial wheels center of gravity defined in the SRF.
- μ: Earth's gravitational constant 398,600.5 $[km^3 s^{-2}]$

2.3 Reference Systems

The Earth Inertial Reference system has the origin at the center of the earth; Z is aligned with the poles from South to North and X pointing toward 0 latitude and 0 longitude.

The Orbital Reference Frame (ORF) is centered on the center of gravity of the entire satellite system (Cubesat body and inertial wheel), has Z aligned with the nadir (e.g. pointing to the center of earth) and X aligned with the velocity vector [See Figure 1].

The Satellite Reference System (SRF) has the origin in the center of gravity of the entire satellite system (Cubesat body and inertial wheel); with the Tate-Bryan angles at zero the SRF coincides with the ORF, [see Figure 2].

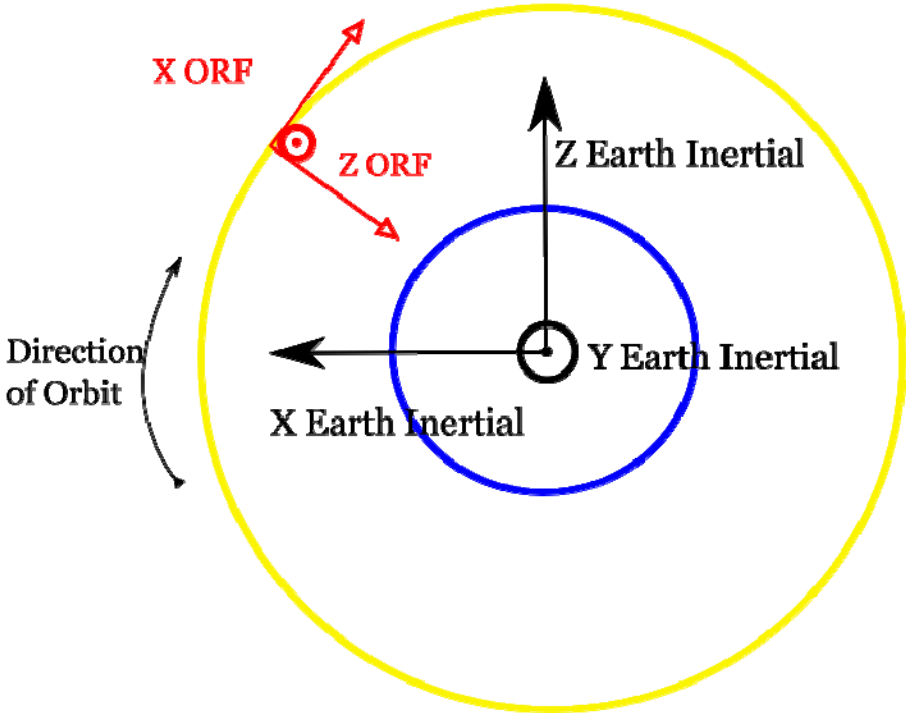

Figure 1: The orbital reference frame

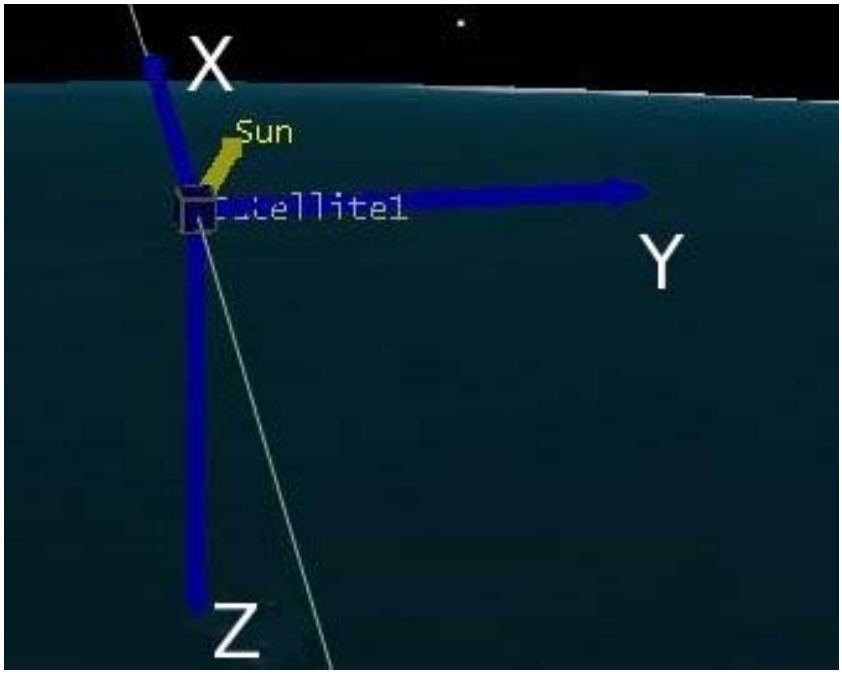

Figure 2: The SRF in zero-zero-zero conditions, equivalent to the ORF

3 PROJECT OBJECTIVES

4 DESIGN REQUIREMENTS

4.1 Dynamical Performance Requirements

The pointing requirement to satisfy the requirements of the science package the ADCS must satisfy. See Swisscube Project Specifications.

Table 1: Dynamical Requirements for ACDS system

Pointing Stability	$0.4^o\,s^{-1}$
Pointing Accuracy	3^o

4.2 Systems and Electrical Performance Requirements

Table 2 Mass and Voltage available for ACDS system

Voltage Available	3.3V
Maximum mass allocated for the ADCS system, including electronics	73 [g]

5 DESIGN ANALYSIS

5.1 Scanning Mode

A critical point which needed definition at the beginning of the project was the scanning mode. We recall that the Swisscube objective is to take measurements of the Night Glow: an atmospheric phenomenon originating from the recombination of oxygen particles at night occurring from 80 to 110 km in altitude.

By Scanning Mode we refer to the attitude strategy with which the satellite scans the earth's atmosphere when taking measurements. The choice of scanning mode strongly influences both the science payload as well as the configuration. The main criteria for choosing the right scanning mode are described in Table 3:

Table 3 Design criteria for the Scanning Mode

1. Pointing Stability: The mode must allow enough time for the Science Payload collect enough

photons to produce a measurement.
2. Pointing Accuracy: The mode must facilitate the determination of the attitude.
3. Atmosphere Limb Pointing: The mode must see through enough of the atmosphere in order to integrate as many photons as possible into the measurements.
4. Systems Integration: The mode must be compatible with possible configurations of the Swisscube components.
5. Complexity: An active scanning mode (e.g. actively moving the science package) must be avoided in order to maintain the simplicity of the attitude control algorithms.
6. Safety: Whenever possible the science package must be shielded from a direct view of the sun to avoid degradation of the optics.

Condition 3 of Table 3 does not allow the science package to be nadir pointed.

The first proposed Scanning mode called for the science package was pointing in the same direction as the orbit (ORF x axis) toward the earth horizon. We refer to this mode as horizon pointing, and it can be seen in Figure 3.

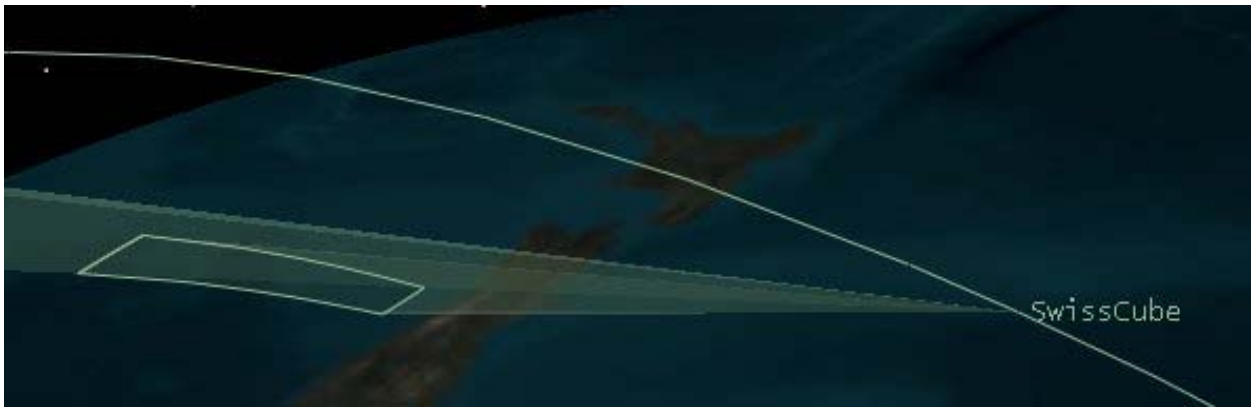

Figure 3: Cubesat forward horizon scanning mode

The Second, and final, scanning mode called for the science package to point in the ORF negative y axis. This mode we refer to as the side-scanning mode and can be seen in Figure 4.

Figure 4: Side-scanning scanning mode

In Table 4 a tabulation of the advantages and disadvantages of the different scanning modes is reported. It is important to note that the inertial wheel is aligned with the SRF x axis, this choice is explained more in detail in § 6.2.3. A more detailed description of a Sun-Synchronous orbit can be found in [Brown].

Table 4 Advantages and Disadvantages of different Scanning Modes

Mode	Advantages	Disadvantages
Horizon Scanning Mode	The earth's horizon provides a clear target for an attitude sensor The mode requires the ADCS system to maintain a constant attitude.	The Science package will point at the sun at least once per orbit. The Inertial Wheel has to be collinear with the axis of the camera.
Side-scanning Scanning Mode	Both the same advantages of the Horizon scanning mode. Since the orbit is Sun-Synchronous in nominal conditions the Science payload will never have a direct view of the sun. Unlike the horizon scanning mode here the inertial wheel is not aligned in the same direction as the science payload but perpendicular to it.	

Both Scanning Modes satisfy Conditions 1 2 and 4 of Table 3. In nominal conditions the Side Scanning mode does shield the science package from the sun. However, in the initial conditions the satellite attitude is uncontrolled. It follows that there is always the possibility of pointing at the sun in either scanning mode. The deciding factor for choosing the Side Scanning mode was that placing the wheel in the same axis as the payload presented significant configuration problems. In fact the initial choice of Horizon Scanning mode forced the wheel to be place directly behind the payload. This created large problems with the fixing of both the wheel and the payload. By choosing the Side Scanning mode the wheel could now be place perpendicular to the payload axis thereby simplifying the internal Cubesat configuration.

5.2 Disturbances

The perturbations, which the satellite must counteract to keep the desired attitude, even in cruise mode, are less significant in space than on earth. Indeed, the gravitational forces are smaller in higher altitude and the friction forces are less present due to the decreasing density of gas particles. Nevertheless, they are an important factor to take into account, and many satellites have a constant spin only in order to minimize the effects of these perturbations. As on earth, the main perturbations in space are the friction forces and the gravitational force, but solar radiation can also create a torque that changes the satellite attitude. These unwanted torques have a direct impact on the accuracy of the pointing direction and on the required power for the actuators. In this section, the torques created by these perturbations are estimated taking at the worst-case scenario.

5.2.1 Solar radiation

The sun continuously emits radiations which applies a force on any exposed surface. The formula of the solar radiation force applied on an area A_s at an incidence angle α can be approximated the following way:

$$F_{rad} = \frac{F_s A_s}{c}(1+q)\cos(\alpha) \approx \frac{3A_s}{c}$$

with c the speed of light ($3 \cdot 10^{-8} m/s^2$), F_s the solar constant ($1.37 W/m^2$) and q the reflectance factor, ranging from 0 to 1. The worst-case approximation can be done by stating that q is 1 and by taking the angle α in the case where it yields the most force, which is when it is equal to 0.

The corresponding torque is simply F multiplied by the distance between the center of gravity and the center of the applied forces, which is roughly the center of the cube:

$$T_{rad} = F(c_{ps} - c_g)$$

The cross-sectional area exposed to the sun is maximal when the sun vector is aligned with a diagonal of the cube. The area is then $A_s = \sqrt{3} \cdot 0.01 \cdot m^2$. Assuming that the center of gravity is off by 2 cm with regard to the geometric center of the satellite, as mentioned in the Cubesat specifications, the disturbance can be estimated:

$$T_{rad} < 10^{-11} Nm$$

5.2.2 Gravity-gradient

Gravity-gradient is used to stabilize some types of satellites with constant orientation with regard to Earth. In order to use these gravity forces, these satellites have asymmetric mass repartition (the moment of inertia along one axis is larger than along any other) so that one axis naturally points down towards Earth. In our case, the disturbances caused by this phenomenon are unwanted, but are also limited thanks to the high symmetry of the Cubesat. The gravity-gradient torque can be calculated by:

$$T_g = \frac{3\mu}{2R^3}\left|I_z - I_y\right|\sin(2\theta)$$

μ is the Earth's gravity constant ($3.986 \cdot 10^{14} m^3/s^2$), θ is the maximum deviation of the z-axis from local vertical, R is orbit radius and I_z and I_y are moments of inertia along z and y. We replace I_y by I_x in the formula if the moment of inertia along x is smaller.

With θ=π/4, R = (6378+400) km and $\left|I_z - I_y\right| = 10^{-1} \cdot kg \cdot m^2$ (value from our early CAD model) and after taking a ten-time margin because of the uncertain values of the moments of inertia, the upper limit of the disturbance can be found:

$$T_g < 2 \cdot 10^{-8} Nm$$

5.2.3 Aerodynamic

This disturbance is far less significant than at ground level, but can nevertheless not be neglected at the orbit of the Swisscube. The aerodynamic force depends on the atmospheric density ϱ, the drag

coefficient C_d, which we can assume to be 2.5 for the Cubesat (we take a small margin from the value of 2.2 given in [Larson et al.]), on the surface area A and on the satellite velocity V. The torque created by this disturbance can be computed following this equation:

$$T_a = \frac{1}{2}\rho C_d A V^2 (c_{pa} - c_g)$$

The center of aerodynamic pressure c_{pa} can be approximated to the center of the cube, and the maximum distance between c_{pa} and c_g is 2 cm then, because the center of mass of the system should not be farther away than 2 cm from the geometric center. The atmospheric density at 400 km is around $10^{-11} kg/m^3$. The velocity is roughly 7 km/s. As explained before for the solar radiation disturbance, the maximum surface area is $A_s = \sqrt{3} \cdot 0.01 \cdot m^2$. With all these quantities, the maximum torque provided by the aerodynamic drag is:

$$T_a < 2 \cdot 10^{-7} Nm$$

5.2.4 Magnetic field

Earth's magnetic field can be used to actuate the satellite, using coils (also called magneto-torquers) that create dipoles that interact with the field. However, this magnetic field can be a disturbance when an undesired residual magnetic dipole is present on the satellite. The residual dipole can be limited by placing the wires properly and making them as short as possible. In the Cubesat designed by Aalborg University [Arnini et al.], the residual dipole was estimated to be around $0.1 \cdot mA \cdot m^2$. The torque depends on the magnetic field, which depends on the altitude:

$$T_m = DB = D\frac{2M}{R^3}$$

M is the magnetic moment of the Earth ($7.96 \cdot 10^{15} \cdot T \cdot m^3$).

With R=6778 km and the aforementioned residual dipole, we can compute the maximum disturbance created by the magnetic field of the Earth:

$$T_m < 6 \cdot 10^{-9} Nm$$

5.3 ACDS Configuration of other Cubesats

The Cubesat Project, led by California Polytechnic State University, started in 1999 with the main objective of creating a standard to facilitate the design and launch of low-cost, very small satellites. On 2003, the first six Cubesat-class satellites were launched into space. In order to take advantage of these previous systems, a review of the ACDS of other pico and nanosatellites was done.

Cubesat	Actuators	Sensors	Remarks
DTUsat (Technical University of	magnetotorquers	Sun sensor, magnetometers	10-degree accuracy, pointing of a fixed

Denmark)			location on the Earth not possible
ION (University of Illinois)	magnetotorquers	magnetometers	10-degree accuracy, 0.12deg/s max rate when pointing, double-Cubesat
AAU (Aalborg University)	magnetotorquers	N/A	8-degree accuracy, wheel not used because of mass concerns
AAUSAT-II	Magnetotorquers, 3 wheels	Gyros, magnetometers, photo-diode (sun sensor)	5-degree accuracy, 0.26deg/s minimum attainable rate, detumbling in 3 orbits (from 0.1rad/s), gyros used to measure the attainable accuracy of the system (not necessary otherwise)

It can be noticed that the required pointing accuracy of previous Cubesats was less stringent than for the Swisscube, and that an inertia wheel may be needed for our system to meet these requirements. The magnetometers are popular due to their good accuracy with respect to their mass and size. One of the AAUSAT-II objectives was to test the capabilities of a system using three inertia wheels, which explains the use of gyros, otherwise not necessary for attitude determination, to test the pointing stability of the system.

5.4 Sensors

The mission of the Swisscube requires an accurate pointing of a camera or a detector to capture a physical phenomenon. In order to determine the attitude of the satellite and decide via the controller how to actuate the satellite for it to point at the desired angle, we need to choose the sensor suite that is to be implemented on the system. There are two main categories of sensors for the three-axis determination of an object in the free space: on one hand, the reference sensors directly detect the angular position of the satellite by comparing it to one or more objects, and on the other hand the inertial sensors yield the angular velocity or acceleration, which has to be integrated to retrieve the attitude. Sun sensors, magnetometers, star sensors, earth or horizon sensors all belong to the first category, whereas gyros measure either the angular velocity or acceleration.

Most of the sensors in the first category allow us to find out the direction of only one observable occurrence with regard to the satellite. For example, sun sensors give out the direction of the sun, or sun vector, and magnetometers detect the magnetic field direction. The major drawback is that it is impossible to establish the three angles that define the attitude of a flying object with either of these sensors, because they only give information about one vector, and the angle around that vector is undefined. To understand this better, let us consider the following example: if the sun vector is perpendicular to one face of the cube, then any rotation along an axis perpendicular to this face will not be perceived by any sun sensors (see Figure 5).

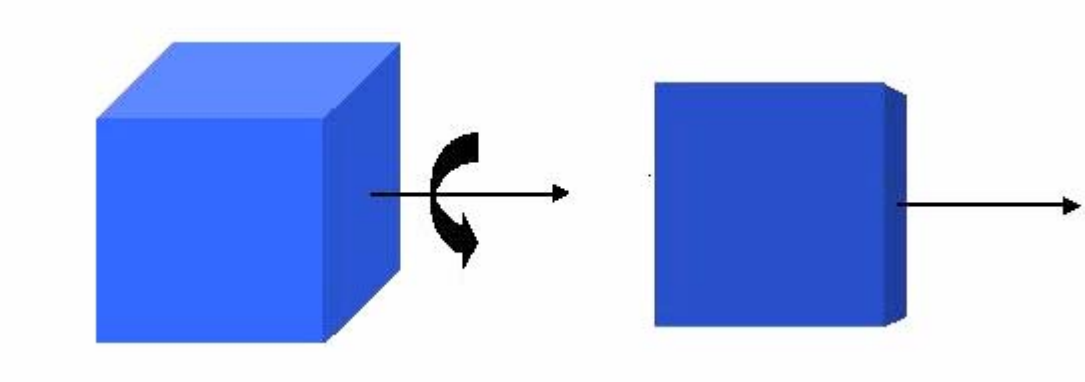

Figure 5: any rotations around the vector are undetected

In order to have all three axes determined, another kind of sensor that detects a non-collinear vector has to be used, like a magnetometer for instance. Indeed, the sun is not aligned with the earth's magnetic field in the general case, and having at least two non-collinear vectors will constraint the three angles. Although horizon sensors can distinguish the tilt of the satellite compared to the horizon, they do not thoroughly determine the attitude of the satellite either, because there is an infinity of possible horizons, like the one on the north and the one on the south, that they cannot differentiate from one another. Thus, most of the angle sensors have a degree of freedom and have to be combined to have a complete information. A notable exception is the star sensor, which can determine from its database of star positions a vector and the tilting around that vector, but at the expense of extensive computational resources.

The gyros functions differently than the aforementioned sensors: they detect the changes in the attitude rather than the attitude itself. Then, their outputs have to be processed and integrated, which means that the initial conditions have to be well known. Hence, they cannot be used alone, and the resulting accuracy depends on the other sensors that define these initial conditions. These can be used in conjunction to a group of sensors presented above to have a more accurate estimation of the attitude during the delay between two of the reference sensors outputs.

There are many criteria we have to take into account when we choose the sensors that are to be on the satellite: their mass, power consumption, power requirements and accuracy are some of them. In the next sections, each type of usable sensor is analyzed.

5.4.1 Sun sensors

Sun sensors are visible light detectors which measure one or two angles (in which case the sun vector is defined) between its frame and the incident sunlight. They are reliable and accurate (up to 0.01 degree accuracy [Larson et al.]), and they require a clear field of view, which might be an issue if the satellite has to constantly rotate to scan the earth. The fact that the Swisscube scientific payload works during the eclipses is another problem: it has to be most accurate when sun sensors are useless. Nevertheless, another type of sensor is needed to have the attitude determined if magnetometers are used, and sun sensors seem to be a good choice considering their mass and simplicity. If an appropriate estimation algorithm is used, such as the Kalman filter, the estimation can still be valid during the eclipse with only partial information.

TNO is working on a small (10x10x2 mm) sun sensor (Figure 6) which accuracy is expected to be around 0.2 degrees. If the Swisscube operating mode is to always point at the horizon without

scanning, the sun sensor can be placed so that it will be exposed to the sunrays for as long as possible.

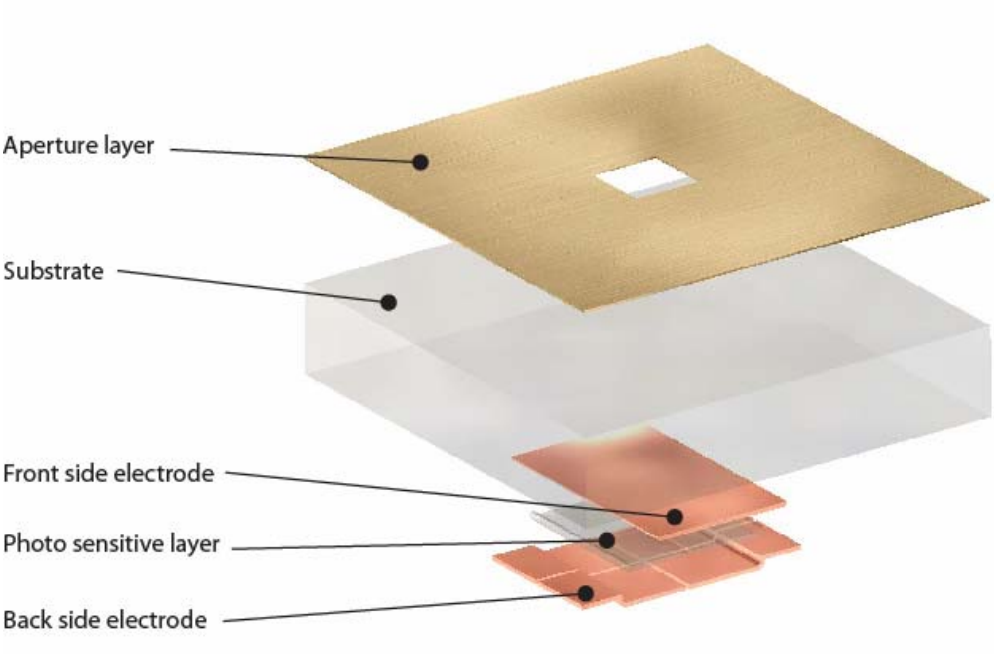

Figure 6: TNO sun sensor

We can also have a cheap, light custom solar sensor by using the solar panels: each panel gives a different power output depending on the incident angle of the sun rays, and the sun vector can be reconstructed using trigonometry. This system is not nearly as accurate as the "real" sun sensors, but it requires nearly nothing, as current sensors at each panel are sufficient to compute the power. The downside is that albedo, the reflection of the sun rays on the Earth, has to be modeled in order to have a decent estimation of the sun vector. This approach has been used by the AAUSAT-II and the Ionospheric Observation Nanosatellite Formation (ION-F). However, problems due to the deterioration of the solar panels over time can occur with this system.

One requirement for the sun vector to be used to calculate the attitude is to have a model of the sun position. The orbit parameters and the time are necessary for that. The sun-synchronous orbit of the Swisscube will make this modeling easier.

5.4.2 Magnetometers

Magnetometers are simple lightweight sensors that measure the magnetic field strength along three axes, and therefore return the magnetic field vector. In low-orbit, they can yield a good accuracy in the order of the degree. The LMIS3 laboratory at EPFL is currently doing research on a small 2D sensor that is to be used as an integrated compass for watches. The idea is to use three of these sensors to have redundant information about the magnetic field vector in the 3D space, which an appropriate estimation algorithm can use to improve the attitude prediction accuracy. Here are the specifications of this sensor:

Mass	2g
Size	10x10x5 mm
Operating voltage	3V
Operating current	3mA
Range	70 µT
Resolution and accuracy	1 µT
Minimum integration time	32 ms (16ms along each axis)
Best integration time	200 ms (100ms along each axis)
Connection	I2C

5.4.2.1 Saturation due to the magnetotorquers

One potential problem with the magnetometers, given that magnetotorquers are the most probable choice of actuators, is that magnetotorquers produce a magnetic field that disturbs the magnetometers. In order to limit this phenomenon, the magnetotorquers and magnetometers have to be as far away from each other as possible. If the contribution of the magnetic actuators does not make the sensors saturate, it is possible to model it and retrieve the Earth's magnetic field. However, even if the actuators are 8 cm away from the sensors, they can cause saturation around the poles, where the field is the strongest, in a 400km orbit. With N=200 coils of area A=100 cm^2 and a current of i=32mA, which are the approximate specifications of the magnetotorquers that are likely to be used on the Swisscube, the field B_x generated by a magnetotorquer at a distance of l=8cm (perpendicularly, i.e. $\theta = \pi/2$, see Figure 7) from it can be approximated by (assuming that the coil is a magnetic dipole):

$$B_x = \frac{2\mu_0}{4\pi}\frac{NiA}{l^3} \cong 25\mu T$$

where μ_0 is the permeability constant ($4\pi \cdot 10^{-7} H/m$).

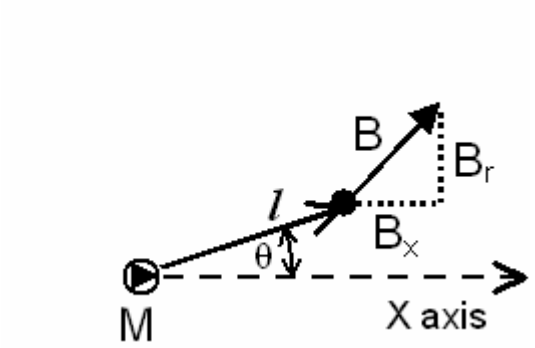

Figure 7: Magnetic field generated by a dipole at a distance l

Thus, if the Earth's magnetic field is greater than 45 µT (the field strength at a 400 km orbit is already of 47.5 µT at Lausanne's latitude), the sensor will saturate if the actuators are used at their

nominal current. If saturation does not occur, the Earth's magnetic field strength can be calculated accurately by subtracting the field generated by the actuators computed by the following equations to the measured field strength:

$$B_x = \frac{\mu_0}{4\pi}\frac{NiA(3\cos^2\theta - 1)}{l^3}$$

$$B_y = \frac{\mu_0}{4\pi}\frac{NiA(3\cos\theta\sin\theta)}{l^3}$$

5.4.2.2 Accuracy of the magnetometer

The angle accuracy obtainable with the EPFL magnetometer can be easily calculated in the 2D case knowing that a measurement along one axis yields an accuracy of 1 µT. The sensor is the least accurate when the field is the weakest and aligned with one axis of the sensor (one axis measurement is zero while the other one is the field strength, see Figure 8). Hence, at an altitude of 400 km, the measured components of a 25 µT field along x may be of 1 µT along y and 24 µT along x, which yields an angle accuracy of 2.4 degrees. At an altitude of 1000 km, the field can be as weak as 16 µT and the resulting accuracy is 3.8 degrees. In a three-dimension space, the obtainable accuracy is roughly the 2D accuracy multiplied by $\sqrt{2}$. Thus, the accuracy that yields this kind of magnetometer is between 3.4 and 5.3 degrees, depending on the orbit altitude.

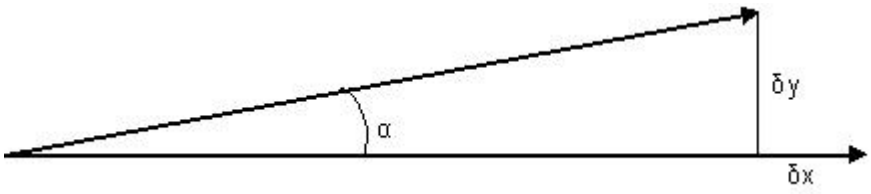

Figure 8: angle error due to the magnetometer accuracy

As long as a good model of the Earth's magnetic field in function of the satellite's position is available, saturation is not necessarily a problem. Indeed, if only one of the three axes along which the measurements are made is saturated, the two remaining measurements and the model can be used to find the missing coordinate (i.e. two components and the modulus of the vector are known and the third component can be found), and the accuracy is nearly not decreased.

If two axes measurements are saturated, the vector cannot be reconstructed, and the resulting accuracy may drop. There is a small possibility that this situation occurs when the field is at its strongest and at a near 45-degree angle between the two axes of a sensor. If the magnetotorquers are actuated at 35 mA at this moment, which is around the maximum input of the currently designed magnetotorquers, both measurements of the sensor will be saturated, i.e. 70 µT, but knowing thanks to a magnetic field model that the field strength can be no more than 65 µT at this position, there is only a small range of angle that the Earth's magnetic field can be in the direction of. Indeed, saturation can occur only when the Earth's magnetic field is greater than 45 µT along one axis, and this can only happen when the angle between this axis and the magnetic field vector is smaller than $\sin^{-1}(\frac{45}{65}) = 46.2°$. The same conclusion can be done for the other saturated axis.

Thus, there is only a range of $2 \times (46.2 - 45) = 2.4°$, centered at 45 degrees, in which saturation can occur on two axes, and the precision is only decreased by 1.2 degree in such a situation. That shows that saturation is not really an issue in our system, because it happens in only special cases and does not lower considerably the accuracy of the attitude prediction. The only requirement is that the Earth's magnetic field has to be known *a priori* by the way of a model, not simply by relying on the output of the magnetic sensors, because this model provides the expected norm of the magnetic field vector.

Nevertheless, saturation can be an important problem if larger magnetotorquers are used and create a stronger field that lowers the 45 µT threshold. A possible solution is to turn off the magnetotorquers when measurements are taken by the magnetometers. However, this is not a very desirable solution, because of the relatively large integration time of these sensors. This can cause some instability, as the controller will not be able to compensate for that amount of time.

As with the sun sensors, a model of the Earth's magnetic field has to be uploaded on the satellite. It is more difficult to model than the sun position, but an interpolation of database that contains up-to-date values can provide accurate results, especially if the lifetime of the system is short, as there is a variation over time of the field.

5.4.3 Star sensors

A star tracker uses a camera (CCD or CMOS) to capture an image of the stars within its field of view and then compares it to its database in order to determine the three-axis attitude of the satellite. It yields the highest accuracy of all the considered sensors (2 arcsec), but it can hardly be used in a Cubesat due to the mass of the camera and the required computational power and memory for image processing. Furthermore, it might not be used for detumbling, because it needs to be relatively still during integration time for the camera to be able to take no blurry images in the dark environment.

5.4.4 Horizon sensors

Horizon sensors have approximately the same configuration as star trackers, but the resolution of the camera can be smaller. The camera can either detect visible or infrared light and tells us if Earth can be seen in the field of view or not. More importantly, at the right angle, it can detect the boundary between Earth and space, the horizon, and thus, two angles with regard to the horizon can be determined.

5.4.5 Gyros

Gyros, or rate sensors, measure the attitude changes and are normally used when the angular rate of the satellite's attitude is high, making numerical differentiation inaccurate.

Many different kind of gyros exist, such as the optical (laser) one, which is usually big and expensive as it measures the frequency shifts, and the piezo-electric vibrating MEMS (micro-electromechanical system), which is the most likely form of gyro to be used in a Cubesat, as it is a small single-chip solution. Because of the nearly constant attitude of the Swisscube, this kind of sensor is unnecessary. They could be used for the detumbling phase with their measurements as control signals, but the requirement of the whole system being shut down before ejection from the P-POD makes this impossible, as when these sensors turn on once in space, they are already rotating and have no information about the attitude rate of the satellite with respect to the Earth.

5.5 Actuators

The choice of the actuators is the integral part of the designing the Swisscube design strategy. The initial analysis of the different actuators reduced the potential choices to three: Magnetic Torquers and Inertial Wheels while the gravity gradient method was also analyzed in depth. The results of the initial analysis and the typical accuracy are reported in Table 5.

Table 5: Recapitulation of results of initial actuator analysis

Actuator	Typical Accuracy,[Larson et al 359]	Results of Preliminary analysis
Spin Stabilization	± 0.1degrees to ± 1 degree	Not adequate for Swisscube
Thruster Systems	No constraints	Not adequate for Swisscube
Gravity Gradient	± 5 degrees	Possible solution
Inertial Wheels	No constraints	Possible solution
Magnetic Torquers	No constraints	Possible solution

5.5.1 Overview and initial analysis of different Actuators

5.5.1.1 Spin Stabilization Methods

These methods such as spin stabilization and dual-spin stabilization were briefly considered as they provide a passive control method for spacecraft attitude. The principle is to use the spacecraft body itself as a gyroscope. A spin stabilized satellite is in fact spined purposely around one of its principal axis in order to increase the gyroscopic stiffness of the two axis parallel to the spin axis.

With good approximation this tenacity can be expressed as, $\omega = \frac{T}{h}$, where h[1] is the angular momentum with which the spacecraft is rotating around its inertia axis and T is a torque perpendicular to the spin axis; the torque will then cause the axis around which the spacecraft is rotating to shift with an angular speed ω [Larson et al, 360]. Recalling the definition of the angular momentum, $h = I\omega_s$, where I is the inertia of the rotation axis and ω_s is the speed with which it is rotating; the equation can be rewritten as:

$$\omega_s = \frac{T}{I\omega}$$

Where ω_s is the spin rotation of the Swisscube body. Taking as a value for a normal Cubesat inertia $I = 2 \cdot 10^{-3} [kg\, m^2]$ and recalling the maximum value for the total disturbances $4.2 \cdot 10^{-7} [Nm]$; we impose that the maximum drift equal to 0.0017 $[\deg / s]$, this value corresponds to around 10 degrees of drift for a 98 minute orbit. This gives the result that the minimum rotation needed is

[1]Noting that the angular momentum h is equal to the product between the inertia and angular rate $h = I\omega$

[3] Respectively the cubesat programs of Aalborg University in the Netherlands, University of Illinois at Urbana-Champaign, Norwegian University of Science and Technology at Trondheim, and Universita degli Studi di Trieste Italy

$405[\text{deg}/s]$. This maximum rotation is over two orders of magnitude higher than the maximum rotation allowed by the science payload.

The dual spin stabilization is also unfeasible due to its complexity in terms of configuration. The dual spin technique previews that the spacecraft have two separate bodies which have constant but different rotational speeds. This technique allows for an active control of the spacecraft attitude; but it requires a more complex configuration. In addition the configuration of the Swisscube does not lend itself to the easy implementation of an independent attitude mechanism for the Science payload, a virtual requirement for a dual-spin stabilization technique; this condition in itself negates the possibility of the implementation of a spin stabilization technique to the Swisscube. For more information on the dual spin see [Wertz].

5.5.1.2 Thruster Systems

This kind of actuator was not considered suitable for the Swisscube system. The need of taking propellant aboard the Cubesat, coupled with the particular thermal and configurations problems of having gas or liquid piping aboard the Swisscube.

An estimation of the size of the system can be made by integrating the disturbances over the minimum duration of the mission. Assuming that we have a couple of 2 thrusters with an arm of $10[cm]$ with respect to each other; in addition we impose that they must provide a torque equal to the maximum disturbance for the minimum duration of the mission. The result is then equal to the ΔV that the propeller tanks must store.

$$\Delta V = \frac{T_{\max} t_{mission}}{0.1[m]}$$

For a 3 month the requirement is $\Delta V = 32\ [m/s]$. One of the possible choices that were looked into for the mission was using an innovative solid propellant cool gas generator thruster system developed between Bradford engineering and TNO labs in the Netherlands. The system offered a ΔV of 4.1 [m/s] with a mass of $130[g]$ only for the tank, and the system already masses more than the mass allocation for the entire ACDS system.

5.5.1.3 Gravity Gradient Stabilization

This method uses the gravity gradient force discussed in § 5.2 as a passive stabilization force. The gravity boom is an element used for passive stabilization. It uses a boom in order to increment the difference between the two inertia axes and by doing so it increments the righting force due to the gravity gradient and keeps the satellite nadir oriented. This method has been adopted by the NCUBE, the NTNU Cubesat program, and proposed for the AtmoCube, University of Trieste Cubesat Program.[Svartveit 16][Ciani 52] This method has the large advantage of being passive but suffers from a considerable weight.

In the Swisscube the possibility of using the gravity boom was studied since the current design previews the need for a 60 cm long antenna attached to one of the faces. The possibility of using this antenna as the initial part of a gravity boom might allow for a considerable reduction in weight of the system as a whole. We do note that according to [Larson et all 363] the accuracy of this system is usually greater than 1 deg. This solution is studied more in depth in §5.5.2.6.

5.5.1.4 Inertial Wheels

By inertial wheels we intend the actuator systems which accelerate a body inside the spacecraft in order to create an equal but opposite force on the spacecraft attitude. Their use is recommended for accuracies lower than 5 degree [Larson et al, 365].

The wheels can be operated in either reaction wheel mode or as a momentum biased system. The first one uses the wheel solely for a reaction torque the second one uses the wheel as a gyroscope in order to increment the rigidity of on particular axis. Both this options are discussed in § 5.5.2.3. The use of one inertial wheel is the baseline design for the Swisscube.

5.5.1.5 Magnetic Torquer

Usually found in either the coil or rod configuration the magnetic torquers are essentially induction coils which are used to create a magnetic field. This induced magnetic field interacting with the earth's magnetic field creates a torque which is then used to change the attitude of the system. This system has the considerable advantage that it is solid state, therefore avoiding the energy losses due to friction. The torque produced however, is proportional to the earths magnetic field which means that they are less effective at higher orbits. [Larson et al 369]

The rod configuration is a configuration that uses wire wrapped around a long rod of ferromagnetic material. The ferromagnetic material increases the efficiency of the coil but greatly increases the weight, this excessive weight the use of rods is not considered for the Swisscube. For the Swisscube the configuration chosen was the coil configuration it is discussed more in detail in §5.5.2.1.

Due to its high applicability to small satellites the magnetic coil this method often used for other Cubesat programs, it has been adopted by the AUUsat, ION, NCUBE, and AtmoCube[3][Frederiksen][Svartveit][Ciani][Gregory]. The method is also used by the newer versions of the Russian TNS small research satellite. A variation using permanent magnets and not induction coils was used by Tokyo University in their Cubesat program.

This attitude stabilization method has one major flaw is that it depends on the cross product between the vector normal of the coil area and the magnetic field strength vector. This means that if both vectors are aligned the produced torque is null. It follows that in every time instant there will be one direction of the Swisscube, the one parallel to the magnetic field, where the magnetic torques will not be able to produce a torque. This introduces non trivial problems to the controllability of the system. The solution adopted by the Swisscube program was to introduce a secondary actuator, an inertial wheel; the inertial wheel produces a torque which does not depend on the direction of the magnetic field. So it can be used to control the axis where the magnetic torquers cannot produce a torque. This problem is discussed more in depth in §5.7.2.

5.5.2 Detailed analysis of chosen actuators

5.5.2.1 Modeling Magnetic Torquers

In 5.5.1.5 the coil configuration was chosen; this configuration foresees that the magnetic torquer will be a coil of multiple turns of metal wire. In Figure 9 we see the schematic of the coils used aboard the Swisscube.

The value that characterizes the magnetic torquers is their magnetic moment whose units is Am^2 and is defined as:

$$M = NIA\vec{n}$$

Equation 1

Where N is the number of turns I is the current and A is the area enclosed by the coil. On the Swisscube there are multiple magnetic torquers, one for every direction, so we define a vector of magnetic moments $M=[M_x, M_y, M_z]$ with $[M_x, M_y, M_z]$ being the magnetic moments associated with the magnetic torquers on the SRF x y and z faces respectively.

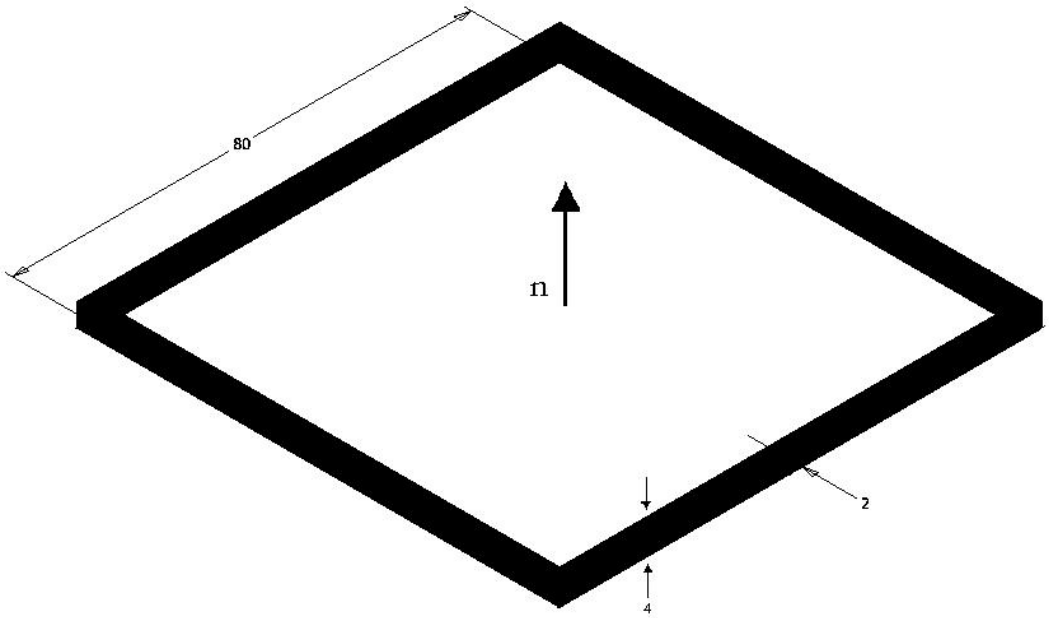

Figure 9: The magnetic torquer coil schematic, Note: all values are in [mm] [Roethlisberger]

The torque produced by the magnetic torquer is the cross product of the magnetic field strength in Teslas, with the magnetic moment of the magnetic torquers.

$$T_{Mag} = \mathrm{M} \times \mathrm{B}$$

Equation 2

Where $B=[Bx, By, Bz]$ Projecting the produced torque in the direction of the magnetic field:

$$\frac{\mathrm{B}}{\|\mathrm{B}\|} \cdot (T_{Mag}) = \frac{\mathrm{B}}{\|\mathrm{B}\|} \cdot (\mathrm{M} \times \mathrm{B}) = 0$$

We find that the producible torque with the magnetic torquer in the direction of the magnetic field is always identically equal to zero, as discussed in § 5.5.1.5. We note that to increment the magnetic moment it is necessary that the area included by the coils be the largest possible. Configuration requirements in the Cubesat defined the coil geometry as an 8 cm cube, see Figure 9.

It is also important to note that Equation 2 can be rewritten as:

$$T_{Mag} = \mathrm{M} \times \mathrm{B} = \overline{\mathrm{B}}\mathrm{M}$$

Where $\overline{\mathrm{B}}$ is a matrix defined as:

$$\overline{B}=\begin{bmatrix} 0 & Bz & -By \\ -Bz & 0 & Bx \\ By & -Bx & 0 \end{bmatrix}$$

This matrix has an identically null determinant, which highlights the problem that the choice of magnetic moments in order to define a torque is not uniquely defined. This analysis can be found in [Ciani].

5.5.2.2 Dimensioning of Magnetic Torquer

In order to dimension the magneto torquers we first define the criterion for dimensioning: The magneto torquers must under the worst possible magnetic field conditions be able to counter act the largest possible disturbance torque.

Initially it is necessary to define the minimum magnetic moment needed, M_N, to counteract the external disturbances. We divide the disturbances and the magnetic moment into two parts; the first is the disturbance due to the residual magnetic dipole and into the ones from other sources, $M_N = M_{NM} + M_{NO}$. To counteract the force due to the magnetic dipole the term due to the magnetic disturbances is set equal to the residual dipole, $M_{NM} = M_R$; the residual magnetic dipole M_R is defined in § 5.2.4.

In order to identify the magnetic moment due to non-magnetic sources it is necessary to choose a reference value for a component of the magnetic field strength, the choice is not immediate since components of the field can be zero. Here the inertial wheel is aligned with the SRF x axis, which in nominal conditions is equivalent to the ORF x axis, assuming that any torques in the SRF x axis can will be controlled by the wheel. This choice leaves to the magnetic torquers the responsibility to control the torques perpendicular to the SRF x axis. Retaking the model in § 5.5.2.1 for the torque due to the perpendicular components of the magnetic torquers we find:

$$T_y = M_z B_x - M_x B_z$$
$$T_z = M_x B_y - M_y B_x$$

The total magnetic field strength is weakest at the equator so using the magnetic field values at that point and adding the condition that all of the magnetic moments are equal $(M = M_x = M_y = M_z)$ we find two equations in 1 unknown.

$$T_y = M(B_x - B_z)$$
$$T_z = M(B_y - B_x)$$

Using the dipole model of the magnetic field we find that at the equator and at nominal conditions where the SRF is equal to the ORF $B_y = B_z = 0$ and $\|B_x\| = \frac{B_0}{R^3}$ with $B_0 = 3 \times 10^{-4}[T]$ and R measured in Earth radii [Larson et al, 212]. This in addition to defining $T_y = T_z = T_{max}$ where T_{max} is the maximum expected moment reduces the system to just one equation.

$$M_N = \frac{B_o}{T_{max} \; R^3}$$

Equation 3

The maximum moment is found at the highest orbit $R = \frac{R_E + 1000km}{R_E}$ with R_E the radius of the earth and for T_{max} equal to the maximum non magnetic disturbances defined in § 5.1, **we note however that for the calculation twice the value for the maximum torque estimated was used**. The results for 400 km altitude are:

Table 6: Estimation of the residual magnetic moment and required magnetic moment for magneto torquers.

System Residual Magnetic Moment	0.001 Am^2
Minimum Magnetic moment needed to counter act the non magnetic disturbances	0.0217
Total Minimum Magnetic Moment	0.0227

Expressing current in terms of consumed power $I=\frac{P}{V}$ and recalling Equation 1 we find that:

$$N_N = \left\lceil \frac{M_N V}{P A} \right\rceil$$

Equation 4

Where M_N is the minimum magnetic moment needed to counteract the disturbances and N_N is the minimum number of turns needed. Recalling the general expression for the resistance of a wire as $R = \frac{\sigma l_w}{A_w}$, where A_w, l_w and σ are the cross-sectional area, the length and σ is the resistivity of the wire material. Substituting $R = \frac{V^2}{P}$ we can rewrite the resistance equation as:

$$A_w = \frac{P\sigma D N_N}{V^2}$$

Equation 5

Where D is the diameter of the magnetic coils. Combining Equation 4 and Equation 5 and defining ρ as the density of the wire material it is possible to find the weight of the magnetic torquers with respect to the available power.

$$m_{Cu} = \frac{P\sigma\rho D^2}{V^2}\left(\left\lceil \frac{M_N V}{P \; A} \right\rceil\right)^2$$

Substituting the the term for resistivity with its expression with respect to temperature $\sigma = \sigma_o(1+\alpha T)$ σ_0 is the resistivity of the material, α is the temperature change coefficient, $\alpha = \frac{d\sigma}{dT}$ and T is the temperature in Kelvin.

$$m_{Cu} = \frac{P\sigma_0(1+\alpha T)\rho D^2}{V^2}\left(\left\lceil \frac{M_N V}{P\ A} \right\rceil\right)^2$$

Equation 6

This however is the weight of the copper wire without isolation. It must be noted that it is imperative that the copper wires be isolated with each other. In order to give an initial approximation of the amount of electrical insulation needed for each wire values for different diameters of available copper wire and their insulation which where already identified by [Fredericksen et all. 32] were taken and linearly interpolated to find the typical insulation needed; the equation is then modified to add the extra mass due to insulation.

$$m_{Tot} = \frac{P\sigma_0(1+\alpha T)\rho D^2}{V^2}\left(\left\lceil \frac{M_N V}{P\ \ A} \right\rceil\right)^2 + m_{iso}$$

In Table 7, we see the values used when calculating the weight of the magnetic torquers. In Figure 10 we can see the necessary weight for the magnetic torquers with respect to the orbit altitude. The mass of the magnetic torquers increments with the temperature because the at higher altitudes the magnetic field is weaker, which means that the magnetic torquers must be able to create a stronger magnetic field in order to create the desired torque. It is important to note the worst case thermal approximation for the temperature on the faces is 303[K] and the magnetic torquers are dimensioned for 340 [K]. This overestimation is done to take into account the local heating of the magnetic torquer coils.

Table 7 Dimensioning properties for the magnetic torquers.

Power Available per Magnetic torquer coil	0.1053 [W]
Available Voltage	3.3 [V]
Maximum Expected Temperature	340 $[K]$
Density (Cu)	8320 $[kg/m^3]$
Resistivity σ_o (Cu)	$1.55\ 10^{-8}\ [\Omega/m^3]$
Temperature Coefficient α (Cu)	$3.9\ 10^{-3}\ [1/K]$
Coil Enclosed area	$6.4\ 10^{-3}\ [m^2]$
Coil Circumference	0.32 [m]

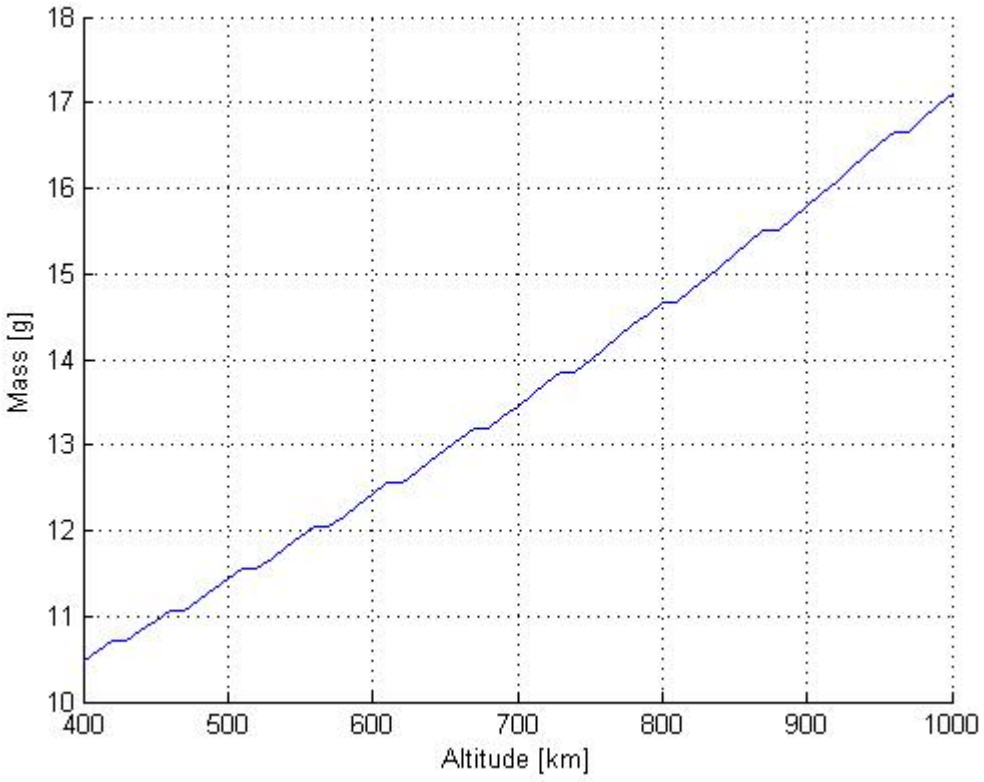

Figure 10: Weight of the magnetic torquer coil with respect to orbit altitude

5.5.2.3 Dimensioning of Inertia Wheel

In this section we analyze two different modes of utilization for the inertial wheel, the first where the sole purpose of the wheel is to reject external disturbances (reaction wheel mode) and the second one is to use the wheel to increment the stiffness of the two axes perpendicular to the wheel rotational axis.

The reaction wheel mode has the advantage that the wheel's nominal speed is zero for most of the orbit; this operating mode has the advantage of consuming less power. While using the wheel to provide a stiffened gyroscopic effect needs for the wheel to have a minimum rotational speed, this means that even if there are no external disturbances the wheel consumes power.

In this section only the dynamical requirements are identified. For requirements we note that the available power is of 100[mW]. The identification of the appropriate motor that satisfies these requirements is not approached.

5.5.2.4 Reaction Wheel Mode

As discussed in § 5.5.2.3 the inertia wheel must be able to withstand the disturbance torques along its axis; this defines what is in fact the minimum force that the engine must be able to project to the inertial wheel. Assuming that all the disturbances are given on the axis of the wheel we define the minimum force output for reaction wheel engine, **we note however, that this value includes a margin factor of 100% (i.e. dimensioned for twice the possible load).**

$$T_{EM} = T_{\max} = 8.4\ 10^{-7} Nm$$

Where $T_{\max}$ is twice the sum of all disturbances found in §5.2. Having defined the minimum force output we now pass to the problem of saturation. One of the main problems of using reaction wheels in space is that the wheel in order to impart a torque on the Cubesat must change its own angular momentum. Since the wheel's mass is fixed the angular momentum is changed by altering the wheel speed.

In a worst case scenario the wheel must continually provide a torque in one direction, this will cause the wheel to continuously accelerate in one direction. Eventually the engine reaches the maximum revolutions pre minute RPM and cannot continue to accelerate the wheel, this condition we refer to the wheel being saturated, and therefore cannot provide further acceleration torque to the satellite. In order to avoid this phenomenon the wheel must be regularly de-spinned, brought back to its nominal speed, in order to maintain a momentum reserve that will allow the wheel to provide further torque.

The de-spinning is achieved by using an auxiliary actuator to create a torque in the same direction as the wheel speed; in this way in order to keep the total torque to zero the wheel speed is reduced. In our specific case with the wheel in the ORF x direction the de-spinning operation can be effectuated close to the poles since in this area the magnetic field of the earth is not aligned with the wheel rotation axis and it is possible for the magnetic torquers to create a torque on the wheel rotation axis , SRF x which in nominal condition is aligned with the ORF x axis.

In order to guarantee that the wheel is never completely saturated it is necessary to quantify the momentum storage that the wheel must internalize each orbit. To do so we consider all forces as secular , in this way assuming that all forces act all the time on the axis, and get the following approximation for the momentum that needs to be stored in one orbit. [Larson et al, Pg 370]

$$h = TP$$

Where P is the orbit period and T is the sum of the maximum torques. Here we do note that for a nadir pointing configuration the gravity gradient is not cyclic but a constant term. In Figure 11 the increased RPM needed each orbit for an orbital period of 105 minutes is shown, it has to be **noted that these values are calculated considering all forces as secular but with no margin factor i.e.** $T_{\max} = 4.2 \cdot 10^{-7}$ **.** We also note that the wheel is assumed as an infinitely thin ring of radius 4[cm] which is very close approximation to the actual inertial wheel on the Cubesat.

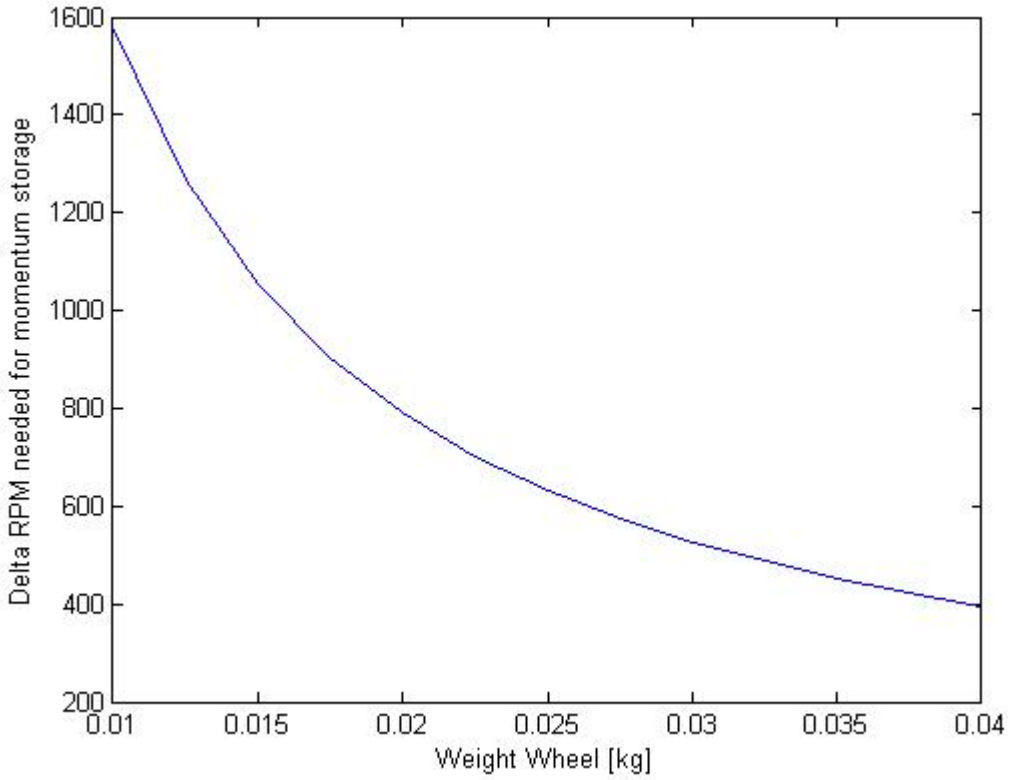

Figure 11: RPM needed per orbit with respect to the weight of the reaction wheel. NOTE: dimensioned with all forces as secular but to the exact value of the maximum torque.

5.5.2.5 Momentum Wheel Mode

Here the wheel is used to guarantee a pointing accuracy in the two axis perpendicular to the wheel rotation axis. We assume that all forces are secular.

$$TP = h\theta_a$$

Where T is the external torque, P is the orbit period, h is the necessary momentum and θ_a is the maximum allowable motion of the axis perpendicular to the wheel rotation axis[Larson et al, 370]. By using the maximum total external torque, magnetic and non-magnetic, found in §5.2, it is possible to find the wheel momentum needed to maintain the necessary attitude. We impose that the satellite using only the momentum wheel must have changed its attitude by a maximum of 3 [deg] $\theta_a = 3[\text{deg}]$, during the duration of the eclipse. So taking $P = 36[\text{min}]$ as the median time of the eclipse and $T = T_{\max} = 8 \cdot 10^{-7}\, Nm$. It is then possible to plot the necessary RPM needed with respect to the available wheel inertia in order to guarantee 3 [deg] precision during the eclipse.

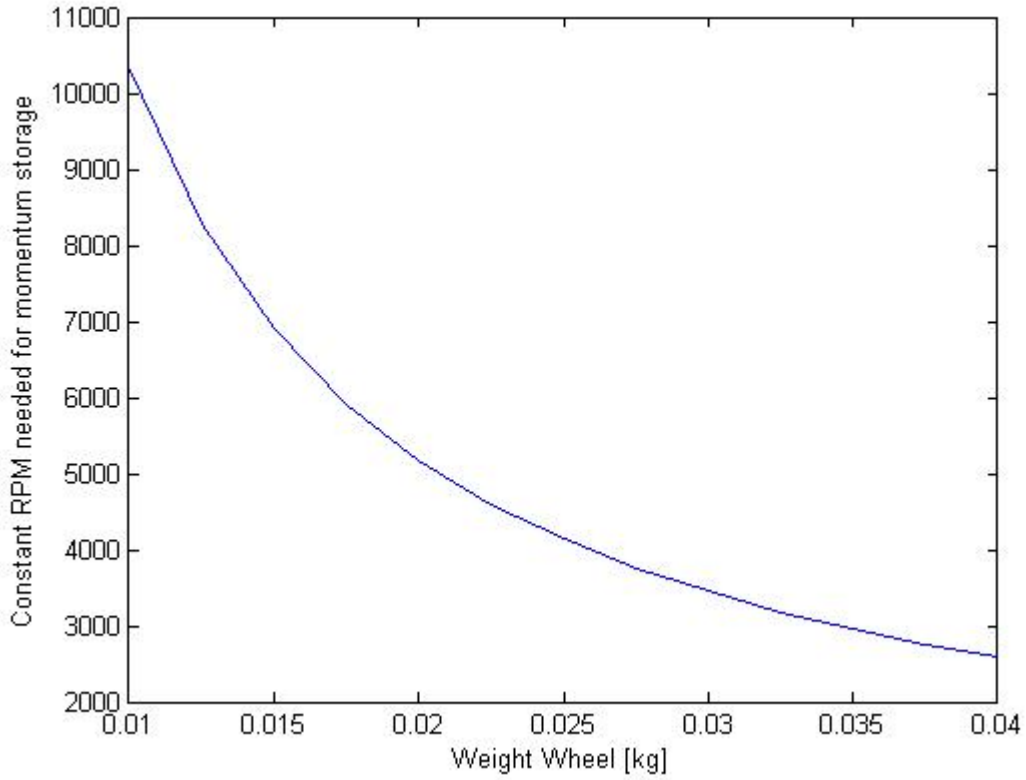

Figure 12: Minimun RPM needed with respect to weight of the momentum wheel in order to maintain 3 degree precision for the duration of the eclipse. NOTE: dimensioned for twice the maximum torque.

5.5.2.6 Dimensioning Gravity Boom

Using the gravity gradient torque identified in § 5.2.2 we rewrite the equation as $T_g = F \sin(2\vartheta)$ Where F includes the terms of the gravity gradient force which do not depend on the rotation angle. Assuming small angles the formula can be rewritten as.

$$T_g = F 2\vartheta$$

Now examining the simplified case where the disturbance force acts upon one axis with Inertia I the previous equation can be rewritten as.

$$\ddot{\vartheta} I + F 2\vartheta = T_d$$

Where T_d is the sum of the maximum disturbance, recalling again that we include a safety factor of 2 i.e. twice the maximum expected, torques not including the gravity gradient and $F2\vartheta$ is the righting moment due to the gravity gradient. The expression is equivalent to that of a forced oscillator. Solving it we find that.

$$\vartheta = -\frac{T_d}{2F}\cos\left(\sqrt{\frac{2F}{I}}t\right) + \frac{T_d}{2F}$$

Equation 7

We now impose the maximum angle , $\vartheta_{\max}$, the satellite can be removed from the zero position. and find the minimum gravity gradient needed $F_{\min\vartheta}$ to maintain the angle within the tolerances.

$$\vartheta_{\max} = \frac{T_d}{F} \Rightarrow F_{\min\vartheta} = \frac{T_d}{\vartheta_{\max}}$$

Equation 8

Finding the derivative with respect to time of the angle:

$$\dot{\vartheta} = \frac{T_d}{\sqrt{2IF}}\sin\left(\sqrt{\frac{2F}{I}}t\right)$$

We now recall the maximum allowable angular momentum for the science package, $\dot{\vartheta}_{\max}$ and we find the minimum gravity gradient $F_{\min\dot{\vartheta}}$ needed to maintain the angular velocity within the tolerances.

$$\dot{\vartheta}_{\max} = \frac{T_d}{\sqrt{2IF_{\min\dot{\vartheta}}}} \Rightarrow F_{\min\dot{\vartheta}} = \frac{{T_d}^2}{2I\dot{\vartheta}^2{}_{\max}}$$

Equation 9

Now testing both needed gravity gradients we find that the condition keep the angle, not the angular rate, is the more stringent condition. We know proceed to calculate the size of the gravity boom needed to stabilize the system.

Since the gravity gradient torque acts only upon I_Z we set: $I = I_z$, T equal to the maximum of all disturbances minus gravity gradient and find the minimum F necessary to maintain the required maximum angular speed. Recalling the formula for the gravity gradient torque it can be found that:

$$F = \frac{3\mu}{2R^3}\left|I_z - I_y\right|$$

Integrating the previous equation with Equation 8 we can find the following relationship between the maximum allowable angle and the inertial difference needed to guarantee it.

$$\left|I_z - I_y\right| = \frac{R^3 T_d}{3\mu\vartheta}$$

Setting $Iz = 2.31 \cdot 10^{-3} [kg\, m^2]$ we find the I_y needed. Setting $I_y = I_{Y_{CS}} + I_{Boom}$ where I_{boom} is the inertia due to the boom and recalling that $I_{Ycs} = 2.6 \cdot 10^{-3} [kg\, m^2]$ it is possible to find the inertia that the boom must add to stabilize the system. Assuming that the boom is composed of thin bar compromising 10% of the weight of the system with a concentrated mass accounting for the remaining 90% of the total mass at the extremity it is possible to plot the total mass of the system with respect to the length of the beam, see Figure 13.

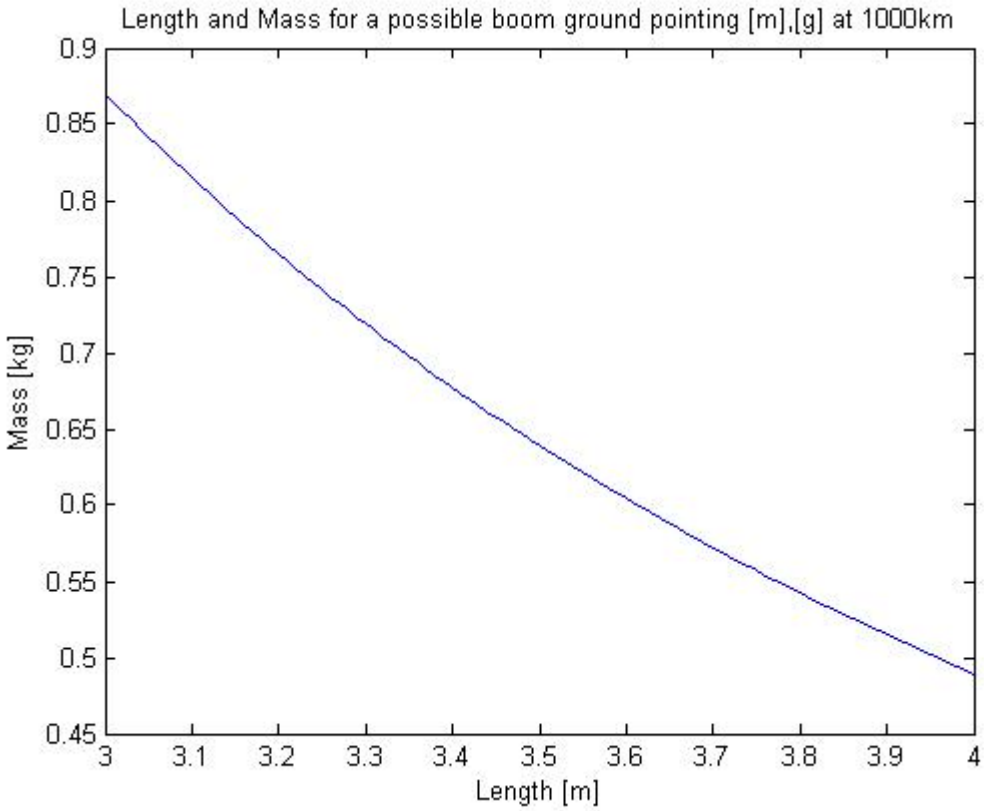

Figure 13 : Mass of gravity boom system with respect to length of beam.

5.6 Dynamic Model

The model was calculate using the Lagrangian approach to calculate the dynamics of the Swisscube with three wheels each attached to one orthogonal face of the Cubesat. The model contains three possible reaction wheels in order to provide the most generality possible at the beginning of the project. However, the reduction of the number of wheels in the model is easily achieved by setting the masses and inertias of the wheel in the model to zero. The convention for naming the wheels is wheel 1, 2 and 3 these being the wheels with rotational axis in the SRF x y and z directions.

While the exposition of the Lagrangian formalism for rigid body dynamics is beyond the scope of this report we note that the formulism is only applicable to inertial reference systems. The attitude of the Swisscube is controlled and calculated in the ORF which is not an inertial reference system. This change brings in the need to add a correction term in the dynamic equations.

The model is resolved by dividing the Swisscube into different rigid bodies parts each with its own associated center of gravity (COG) and inertia matrix. **We separate the wheels from the**

Swisscube structure treating each wheel as a separate rigid body. **We note that in this section the by Cubesat body we intend the Swisscube without the inertial wheels**. At this point we have four separate rigid bodies with 4 separate COG and Inertia Matrixes. Also noting that the coupling between the wheel and the Cubesat body equations is achieved by the common rotational and translation terms discussed in § 5.6.1.1 and 5.6.1.2 as well as by the common term due to the engine action discussed in §5.6.3 it is important to clarify that the ORF has its origin in the COG of the entire system and is therefore the Instantaneous center of rotation for all points solidary to the system rigid body.

The generalized coordinates, q, used were the Tate-Bryan Angles as well as the angular positions of the wheels: $q = (\phi, \theta, \psi, \varphi_1, \varphi_2, \varphi_3)$. The Tate-Bryan Angles are a particular kind of Euler angles which follow a 1-2-3 rotation order. It should also be noted that the generalized coordinate due to the wheels φ_1, φ_2 and φ_3 are cyclic and could be suppressed, however, for the simplicity of the analysis all the coordinates will be treated equally.

For a more in-depth treatment of Euler Angles an explanation in included in [Wertz]. We do note however that Euler angle representation contains a singularity, sometimes known as gimbal lock. While in nominal attitude conditions this does not present a problem, it should be kept present when using the model. We also note that all the symbols and their meanings are defined in § 2.

5.6.1 Kinematics

5.6.1.1 Rotational Speeds

The rotational speed of a solid body whose attitude in 3-space is defined by use of Tate-Bryan angles in the BRF can be expressed as the rotation induced by each angle variation in the direction of the unit vector associated with it.

$$\Omega = (\omega_x, \omega_y, \omega_z) = \dot{\phi}\,\hat{x}_o + \dot{\theta}\,\hat{y}'_o + \dot{\psi}\,\hat{z}_s$$

Equation 10

With $\hat{x}_o$ the ORF x axis, and $\hat{z}_s$ the SRF z axis. Also, $\hat{y}'_o$ is the y axis of the first intermediate reference system created immediately after the rotation of the ϕ coordinate around $\hat{x}_o$. By projecting the intermediate $\hat{y}_o{}'$ vector into the SRF it is possible to prove that:

$$\hat{y}'_o = (\cos(\phi) \quad R \quad \hat{y}_o + \sin(\phi) \quad R \quad \hat{z}_o)$$

Equation 11

The term R is the rotational matrix from the ORF to the SRF which for the case of for Tate-Bryan Euler angles is equal to:

$$R = \begin{bmatrix} \cos(\psi) & \sin(\psi) & 0 \\ -\sin(\psi) & \cos(\psi) & 0 \\ 0 & 0 & 1 \end{bmatrix} \begin{bmatrix} \cos(\vartheta) & 0 & -\sin(\vartheta) \\ 0 & 1 & 0 \\ \sin(\vartheta) & 0 & \cos(\vartheta) \end{bmatrix} \begin{bmatrix} 1 & 0 & 0 \\ 0 & \cos(\phi) & \sin(\phi) \\ 0 & -\sin(\phi) & \cos(\phi) \end{bmatrix}$$

.

Having defined the rotational speed of a body in 3-space we now define Ω_{CS} as the rotational speed of the satellite body in the SRF and proceed to project $\hat{x}_o$ and $\hat{y}'_o$ in the SRF, the Ω_{CS} expressed in the SRF can be expressed as:

$$\Omega_{CS} = \dot{\phi} \;\; R \;\; \hat{x}_o + \dot{\theta} \;\; (\cos(\phi) \;\; R \;\; \hat{y}_o + \sin(\phi) \;\; R \;\; \hat{z}_o) + \dot{\psi} \;\; \hat{z}_s + \;\; R\Omega_{OR}$$

Equation 12

With the term Ω_{OR} is the rotational speed of the ORF expressed with respect to the earth inertial reference system expressed in the SRF, this term is added to take into account the fact that the ORF is not an inertial reference frame and is rotating with a given rate. The rotational speed in the ORF defined by the ORF is equal to $\Omega_{OR} = [0, -\omega_{OR}, 0]$ with $\omega_{OR} = \sqrt{\frac{\mu}{r^3}}$; where $\mu = 3.986 \cdot 10^{14} [m^3 s^{-2}]$ and r is the orbit radius in meters.[Larson et al, 380]

Solving Equation 12 we can derive the following expression:

$$\Omega_{CS} = \begin{bmatrix} \dot{\phi}\cos(\psi)\cos(\vartheta) + \dot{\vartheta}\sin(\psi) \\ -\dot{\phi}\sin(\psi)\cos(\vartheta) + \dot{\vartheta}\cos(\psi) \\ \dot{\phi}\sin(\vartheta) + \dot{\psi} \end{bmatrix} + \omega_{OR} \begin{bmatrix} -(\sin(\psi)\cos(\phi) + \cos(\psi)\sin(\vartheta)\sin(\phi)) \\ -(\cos(\psi)\cos(\phi) - \sin(\psi)\sin(\vartheta)\sin(\phi)) \\ \cos(\vartheta)\sin(\phi) \end{bmatrix}$$

Having defined the rotational speed of the Cubesat we now define the rotational speed of the inertial wheels. Since the wheels are solidary with the cubesat body their rotational speeds is composed of the cubesat body rotational speed plus the added term due to the wheel rotation.

$$\Omega_{W1} = \Omega_{CS} + \dot{\varphi}_1 \hat{x}_s$$
$$\Omega_{W2} = \Omega_{CS} + \dot{\varphi}_3 \hat{y}_s$$
$$\Omega_{W3} = \Omega_{CS} + \dot{\varphi}_2 \hat{z}_s$$

5.6.1.2 Translational Speed of the COG of the Cubesat body and the inertial wheels

Recalling that the speed of a point in a rotating body is $V=\Omega\times(P-O)$ where O is the instantaneous center of rotation. For a non constraint body the instantaneous center of rotation is it global center of gravity. Since the different wheel COG are solidary to the cubesat system. Then the translational speeds of the centers of gravity of the Cubesat body and the wheels can be expressed as:

$$V_{CS} = \Omega_{CS} \times P_{CS}$$
$$V_{Wi} = \Omega_{CS} \times P_{Wi} \text{ with i = 1, 2, 3.}$$

Where P_{CS} and P_{Wi} are the position vectors in the ORF from the ORF origin to the COG of the different rigid bodies, cubesat body and the inertia wheels.

5.6.2 Kinetic Energy

Defining the kinetic energy T of the cubesat body as T_{CS} and of the three inertial wheels as T_{W1}, T_{W2} and T_{W3}. Recalling that the kinetic energy of a body calculated with respect to its center of gravity is equal to $T = \frac{1}{2}\Omega^T I\Omega + \frac{1}{2}V^T MV$; where Ω is the rotational speed, I is the inertia matrix, V is the velocity of the COG and M is the mass. It is then possible to define the kinetic energies of the cubesat body and the wheels.

$$T_{CS} = \frac{1}{2}\Omega_{CS}{}^T I_{CS}\Omega_{CS} + \frac{1}{2}(\Omega_{CS} \times P_{CS})^T M_{CS}(\Omega_{CS} \times P_{CS})$$

$$T_{WE} = \frac{1}{2}\Omega_{Wi}{}^T I_{Wi}\Omega_{Wi} + \frac{1}{2}(\Omega_{CS} \times P_{Wi})^T M_{Wi}(\Omega_{CS} \times P_{Wi}) \text{ with i=1,2,3}$$

5.6.3 Work of the Generalized Forces

The work of the generalized forces δW is defined as:

$$\delta W = \sum F \square e_i \delta q_i$$

Equation 13

Where e_i is the unit vector associated to each generalized coordinate. We proceed by calculating separately the virtual work due to forces acting on the cubesat body and the virtual work due to forces acting on the reaction wheels.

The treatment of the wheels requires some extra considerations. **It must be noted that all external forces are modeled as acting only on the cubesat body, while the sole working torque is considered as acting on the inertial wheels is the torque due to the wheel motor.** This is a direct consequence of the decision to treat the Cubesat structure and the wheels as separate rigid bodies. Analyzing the forces on the Swisscube body we see that both the external forces and the torque from the inertial wheel work on the Tate-Bryant angle coordinates (ϕ, θ, ψ). So the work done on the attitude coordinates (ϕ, θ, ψ) is the sum of the work done by the external forces and the work done by the inertial wheel's motor. However, for the wheels the only non-constraint force which has an allowable virtual work is the torque of the engine.

Also, since the two bodies are treated separately the terms of the torque due to the wheel engines is in fact expressed twice: once as the force that the engine acts upon the wheel and also as the reaction force done by the wheel on the cubesat body. In fact this double term is necessary to the system as it provides one of the main coupling terms between the cubesat structure dynamics and the inertial wheel dynamics.

We begin by defining the forces acting on the cubesat body expressed in the SRF. The first torque considered is the torque due to the magnetic torquers defined in §5.5.2.1.

$$T_{Mag} = \mathrm{M} \times \mathrm{B} = [T_{MagX}, T_{MagY}, T_{MagZ}]$$

Equation 14

We now define the torque produced by the inertia wheel's motors on the cubesat body:

$$M_{we} = [M_{we1}, M_{we2}, M_{we3}]$$

For a positive torque the inertia wheel motors produce a positive rotation of the wheel generalized coordinates $(\varphi_1, \varphi_2, \varphi_3)$. The cubesat body itself receives the reaction torques from the acceleration of the inertial wheels. This extra added term is the attitude control torque which allows us to act, through the inertia wheels, upon the attitude of the cubesat.

Now defining the sum of the disturbance torques due to external factors, see §5.2 for a more detailed explanation, as: $T_D = [T_{Dx}, T_{Dy}, T_{Dz}]$

We now define the sum of the torques acting upon the cubesat body as $T_{TotalCS}$.

$$T_{TotalCS} = T_{Mag} + T_D - M_{we}$$

Equation 15

Noting that the negative sign is due to the fact that M_{we} is the reaction torque from the inertia wheel motors; in other words since a positive M_{we} creates a negative change in the cubesat body angle and vice-versa their produced work will always be negative.

Recalling that the generalized coordinates for the cubesat are the Tate-Bryan angles and that the rotational speed in Equation 12 were defined as the time variations of the angles multiplied by their associated unit vectors. In fact Equation 12 , ignoring the $R\Omega_{OR}$ term, can be rewritten as:

$$\Omega = \sum e_i \dot{q}_i$$

Taking advantage of this similarity between this expression and Equation 15 it is possible to express the work due to the external force of the generalized forces as:

$$\delta W_{CS} = T^T{}_{TotalCS}(\delta\phi R\,\hat{x}_o + \delta\theta(\cos(\phi)R\hat{y}_o + \sin(\phi)Rz_o) + \delta\psi\,\hat{z}_s)$$

The expression of the work of the generalized forces on the wheels is simpler; recalling that the moment of the wheel engine creates a positive change in the generalized coordinates for the wheels then it is possible to rewrite the virtual work of the generalized forces as:

$$\delta W_{Wheels} = M_{We1}\delta\varphi_1 + M_{We2}\delta\varphi_2 + M_{We3}\delta\varphi_3$$

Summing both the work of the generalized forces on the cubesat body and the work of the generalized forces on the wheels we can find the work of the generalized forces for the entire system, cubesat body plus inertial wheels.

$$\delta W_{Total} = \delta W_{CS} + \delta W_{Wheels}$$

5.6.4 Resolution of the Lagrangian formalism

Recalling that the Lagrangian function is defined as the difference between the kinetic and potential energy terms.

$$L = T - V$$

We note that although it might be possible to define a potential energy due to the difference in angle between the magnetic field and the normal of the magnetic torquers. However, in this analysis I choose to represent the effect of the magnetic torquers as external forces. So the total lagrangian function we can define as:

$$L = T_{CS} + T_{WE}$$

Applying the functional of the lagrangian formalism:

$$\frac{d\partial L}{dt\partial \dot{q}} - \frac{\partial L}{\partial q} = \frac{\delta W}{\delta q}$$

Equation 16

With $q = \phi, \vartheta, \psi, \varphi_1, \varphi_2$ and φ_3 it is possible to find the 6 scalar second order non-linear differential equations that define the dynamics of the system.

5.6.5 Linearization of the System

In order to be able to apply the results of classical linear, time, invariant, and null initial condition systems theory it is possible to define a linearized approximation of the system. In order to define the linear systems we first define nomenclature.

It is possible to rewrite the equations resulting from Equation 16 in the following form:

$$\dot{\vec{x}} = F(\vec{x}, u)$$

Where $\dot{\vec{x}}$, in the case of only one inertial wheel, is equal to $\dot{\vec{x}} = [\phi, \dot{\phi}, \vartheta, \dot{\vartheta}, \psi, \dot{\psi}, \varphi_1, \dot{\varphi}_1]^T$ and $\vec{u}$ is the entry of the system, again in the case of one wheel $\vec{u} = [M_x, M_y, M_z, M_{Wel}]^T$ .Then defining the linearization position constant vectors $\vec{x}_o$ and $\vec{u}_o$ and imposing that $F(\vec{x}_o, \vec{u}_o) = 0$ the original dynamical system can be rewritten as:

$$\dot{\tilde{x}} = \left.\frac{\partial F}{\partial x}\right|_{(\vec{x}_o, \vec{u}_o)} \tilde{x} + \left.\frac{\partial F}{\partial u}\right|_{(\vec{x}_o, \vec{u}_o)} \tilde{u} = A\tilde{x} + B\tilde{u}$$

Where $\tilde{x} = x - x_o \; and \; \tilde{u} = u - u_o$. We note that since our system takes into input the magnetic moments, whose resulting torque is a function of the magnetic field, the B matrix is not constant but a function of the magnetic field. However, in this report the model is linearized by inputting a constant value for the magnetic field.

5.7 Controllability and Open-loop stability

We know analyze the stability and controllability of the system. Initially we see that the Swisscube attitude is in fact unstable if not controlled and therefore requires a controller. In order to better place direction of the wheel we perform a controllability analysis of the system. The first approach involves analyzing the controllability of the linearized system around the nominal conditions $\phi = 0, \theta = 0$ and $\psi = 0$. The results that prove that the system is in fact globally controllable are also reported.

5.7.1 Open loop stability

In order to determine the open-loop stability of the system the eigenvalues of the linearized system dynamic matrix were analyzed, these are reported in Table 8. We note that these are equivalent the system poles. We do see that there is at least one, in fact there are four, eigenvalues with a positive real component. Therefore, the conditions for stability of the system are not satisfied. The system

requires an active stabilization in order to be controlled. This **imposes the need of an active control system on the Swisscube**. This result however was expected, due to the numerous non-damped gyroscopic effects present in the space environment.

Table 8: Eigenvalues of the open loop system.

$$eig(A) = \begin{Bmatrix} 0 \\ 1.4\cdot10^{-6}+0.001\mathrm{i} \\ 1.4\cdot10^{-6}-0.001\mathrm{i} \\ 2.4\cdot10^{-5}+0.0002\mathrm{i} \\ 2.3\cdot10^{-5}-0.0002\mathrm{i} \\ -3.6\cdot10^{-5} \\ -1.6\cdot10^{-5} \\ 1.9\cdot10^{-8} \end{Bmatrix}$$

5.7.2 Linearized Controllability

In order to start defining the ACDS configuration for the Swisscube it was necessary to define the controllability of the resulting system configuration. In the controllability analysis we define 5 different possible configurations, see Table 9 Possible Inertial Wheel configurations for the Swisscube.

Table 9 Possible Inertial Wheel configurations for the Swisscube

Configuration 1	One inertial wheel normal to $\hat{x}_{OR}$ and three magnetic torquers
Configuration 2	One inertial wheel normal to $\hat{y}_{OR}$ and three magnetic torquers
Configuration 3	One inertial wheel normal to $\hat{z}_{OR}$ and three magnetic torquers
Configuration 4	Three inertial wheels each normal to $(\hat{x}_{OR}, \hat{y}_{OR}, \hat{z}_{OR})$ and three magnetic torquers
Configuration 5	Three magnetic torquers and no wheels.

We now calculated controllability of the system by defining the controllability matrix **C**, defined as:

$$C = \begin{bmatrix} B & AB & A^2B & .... & A^{n-1}B \end{bmatrix}$$

Equation 17

Where $A \text{and} B$ are the matrixes of the linearized system as discussed in §5.6.5. If the rank of the controllability matrix is greater than or equal to n then the system is controllable [Gillet]. In order to test the controllability of the linearized system in the different configurations we define a test case orbit going from 90S to 90N along the prime meridian at an altitude of 600km.

Starting by Configuration 5 , only magneto torquers, linearizing around the equator it results that the rank of the controllability matrix is equal to the rank of the system, therefore defining the system as

uncontrollable. This is a unexpected result since in section § 5.5.2.1 it was seen that with only magnetic torquers it is impossible to create a moment the axis parallel to the magnetic field therefore there exists one axis where there is no possibility of active control. However, a closer examination of the controllability matrix shows that its conditioning number is $3.017 \cdot 10^8$ which is excessive, this is an indication that the matrix's columns are very close to being linearly dependent; a probable physical explanation for the phenomenon is that the gyroscopic effects due to the rotation of the ORF gives a slight coupling with the uncontrollable axis. Since the coupling is very weak it is possible to conclude that the system without an inertial wheel is effectively instantaneously uncontrollable a secondary propulsion system is needed.

Testing configurations 1, 2, 3 and 4 for different latitude positions we see that they are all controllable with different condition numbers, see Table 10. The condition number for the controllability of Configuration 2 is much higher than the other configurations and is disregarded immediately. Configuration 4 gives the best controllability but however its weight is prohibitive, which leaves Configuration 1 and Configuration 3 as roughly equivalent possible choices.

Table 10: Mean Condition number over half an orbit for different inertial wheel configurations

Configuration 1	$8.4 \cdot 10^6$
Configuration 2	$2.04 \cdot 10^8$
Configuration 3	$4.4 \cdot 10^6$
Configuration 4	$4.1 \cdot 10^6$
Configuration 5	$3.017 \cdot 10^8$

5.7.3 Global Controllability

While in § 5.5.2.1 it has been seen that the system is not instantly controllable with only the magnetic torquers. This was due to an uncontrollable axis parallel to the magnetic field. However the system is only instantly uncontrollable. It can be proven that the system is in fact strongly accessible and controllable [Bhat]. This proof is beyond the scope of this report but for reference the results are synthesized.

The controllability is mainly due to the fact the magnetic field can be in fact modeled as a time dependent sinusoidal function; this brings the requirement that the must not be in a equatorial orbit since this orbit the magnetic field direction is approximately constant[Bhat]. An interpretation of these results if that if the magnetic field direction changes over time then in fact the magnetically uncontrollable axis of the system also changes, it follows that over a period of time all of the axis of the system are controllable. The Swisscube is in a polar orbit so the condition well satisfied.

5.8 Controller

The choice of the control strategy for the Swisscube is not immediate. In Table 10 we see the possible steps, from the ADCS perspective that will bring the satellite into the nominal control conditions the complete timeline can be found in [Despont]. By nominal conditions we intend the

satellite in a stable attitude with the payload pointing towards the limb. The conditions for this require that the payload be rotated between 17 to 29 degrees downward.

Table 11 Timeline of the controller

1. Expulsion from the P-Pod, rotation at 0.1 $[rad\ s^{-1}]$
2. Start ADCS system, antenna deployment
3. Begin de-tumbling controller
4. Receive data from ground station with orbital and position parameters
5. Begin attitude determination
6. When de-tumbling controller has reached equilibrium begin nominal control

Table 10 highlights an important part of the control strategy, there are in fact 2 different control systems the first is the de-tumbling control the second is the nominal control.

5.8.1 Detumbling Control

The de-tumbling controller is activated in the initial phase of the system. The main objective of the controller is to decrease the kinetic energy of the system while bringing the system as close as possible to the nominal conditions. There are numerous possibilities for implementing this controller.

An often used control law is the $\dot{B}$ control law. Here the control system uses a simple feedback controller in order to bring the variation of the magnetic field vector direction $\dot{B}$ to zero. This control strategy has the advantage that it can be implemented as a non state-based controller, and so does not require any attitude determination to continue. Another possibility is the $\dot{S}$ control law where the variation of the angle of the sun vector is used in the place of the magnetic field strength. This law has the disadvantages that during the eclipse it is not possible to determine the direction of the sun vector.

During this project the problem of the de-tumbling control was not approached. Its determination and implementation are however important tasks for the future.

5.8.2 Nominal Control

The nominal control is the controller that controls the satellite in the normal flight coordinates. The main problem for the implementation of the nominal control is the strong nonlinearity of the magnetic field. The creation of the global non-linear control is beyond the scope of the Phase A we do note however that the problem has already been studied; in fact a possible type of time varying controller applied to magnetic actuation can be found in [Lovera et al].

For this phase Swisscube project we developed a possible control algorithm for the nominal conditions. This algorithm is based on an optimal control, linear-quadratic regulator, based on the linearized dynamical model. We note that in the simulations the attitude determination is assumed ideal, the controller has perfect knowledge of all states. In this section we will present a first iteration of a linearized control algorithm.

5.8.2.1 Parameters of the controlled system.

The system is a 8th order system. Defining the state vector x:

$$x = \{\dot{\phi}, \phi, \dot{\theta}, \theta, \dot{\psi}, \psi, \dot{\varphi}_1, \varphi_1\}$$

The system is in fact MIMO for the purpose of the controller simulation it is assumed that the controller has access to the current values of all the states. For the input states we define an input vector u defined as:

$$u = \{M_x, M_y, M_z, T_{w1}\}$$

Where M_x, M_y *and* M_z are the magnetic moments associated with the three magnetic torquers, see § 5.5.2.1, and T_{w1} is the torque applied by the inertial wheel engine on the inertial wheel.

5.8.2.2 Controller Linearization Position

The main problem of designing the controller is that the direction of the earth's magnetic field is not constant with respect to the ORF, see Figure 14.

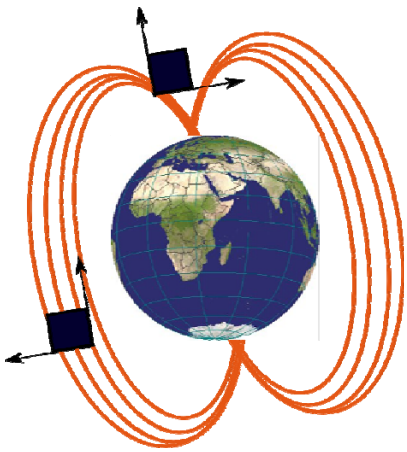

Figure 14: The Magnetic field of the earth with respect to the satellite position.

This means that there since the local conditions vary greatly for position to position it is not advisable to create a global linear controller that will work effectively at all times system. For this Phase a linear controller was created to stabilize the system in the vicinity of the equator in nominal conditions. We note thought that for simplicity in this tentative controller we study the case where the values are brought down to zero.

Table 12: Controller linearization positions

$$\text{State Variables: } \phi = 0, \dot{\phi} = 0, \theta = 0, \dot{\theta} = 0, \psi = 0, \dot{\psi} = 0, \varphi_1 = 0 \text{ and } \dot{\varphi}_1 = 0$$

$$\text{Magnetic Field in ORF: } B_x = 0.3 \cdot 10^{-4}[T] B_y = 0 \text{ and } B_z = 0$$

The values used for the inertias and positions of the different bodies used can be found in Appendix C**Error! Reference source not found.**.

5.8.2.3 Controller Synthesis

The method chosen to stabilize the satellite was the linear-quadratic regulator optimal controller. Recalling that the linear-quadratic regulator emphasis is in the minimization of the following cost function:

$$J = \int \left(x^T Q_1 x + u^T Q_2 u \right) dt$$

Where the matrixes Q_1 and Q_2 permit a compromise between the control and the contribution of different actuators to the system control. In this controller to dimension the matrices Q_1 *and* Q_2 as a starting point the empirical rule reported by [Frederiksen et al, 50] was used it is reported below:

$$Q_{1(i,i)} = \frac{1}{\overline{x}_{iMax}^2} \text{ and } Q_{2(i,i)} = \frac{1}{\overline{u}_{iMax}^2}$$

For Q_1 and Q_2 the empirical law provided a starting point but the parameters were later adjusted.

In order to maximize the response to the Cubesat attitude state variables Q_1 matrix was designed as a diagonal matrix with the first 6 values, those associated to the CS attitude variables angles having a value of 0.4 their angular derivatives 25 and the two values related to the wheel were set to 10^{-20}. For the magnetic torquers the weight assigned to them was 5 for the inertial wheel its value is $1.4 \cdot 10^3$, the weights used for the matrix resumed in Equation 18.

While these weights allowed the controller to effectively reject the inputs the weights give rise to almost singular matrices, especially in the case of Q_1. This gives creates a problem with the solution of the Riccati equation. In fact the current weights are close to the numerical limit to effectively solve the Riccati equations. While the controller has responded well in tests this numerical sensitivity of the solution should be kept in mind.

$$Q_1 = \begin{bmatrix} 0.4 & & & & & & & & & & & \\ & 25 & & & & & & & & & & \\ & & 0.4 & & & & 0 & & & & & \\ & & & 25 & & & & & & & & \\ & & & & 0.4 & & & & & & & \\ & & 0 & & & & 25 & & & & & \\ & & & & & & & 10^{-20} & & & & \\ & & & & & & & & 10^{-20} & & & \\ & & & & & & & & & & & \end{bmatrix} \qquad Q_2 = \begin{bmatrix} 5 & & & & 0 \\ & 5 & & & \\ & & 5 & & \\ 0 & & & & 1400 \end{bmatrix}$$

Equation 18

Having Q_1 and Q_2 it is possible to calculate the feedback gain matrix K; where $u = -Kx$ is the new input for the dynamical system with x the state vector. We do note that for the controller the last 2 columns of the feedback gain matrix K where forced to zero, in order to avoid correcting for wheel position and speed. This is fact equivalent to forcing the error on the wheel position and speed as zero, the matrix used is reported below.

$$K = \begin{bmatrix} 0 & 0 & 0 & 0 & 0 & 0 & 0 & 0 \\ 6.5\cdot10^{-4} & 4.8\cdot10^{-3} & -5.6\cdot10^{-6} & 2.3\cdot10^{-4} & -0.30 & -2.2 & 0 & 0 \\ 5.2\cdot10^{-3} & 3.9\cdot10^{-3} & 0.30 & 2.2 & 5.9\cdot10^{-6} & 2.3\cdot10^{-4} & 0 & 0 \\ -1.8\cdot10^{-2} & -0.13 & 3.1\cdot10^{-4} & 2.3\cdot10^{-3} & 3.9\cdot10^{-5} & 2.9\cdot10^{-4} & 0 & 0 \end{bmatrix}$$

Equation 19

In order to validate the choice of forcing the last two columns of K to zero we check if the poles of the feedback system as a whole are stable. By computing the eigen-values of the feedback system matrix $eig(A-B\cdot K)$ we find them in Table 13. We see that all values are real and negative or null. It follows that the controlled system in stable. We do note however that this results utilizes the linearized dynamic model matrices A and B while the controller is implemented to the real non-linear system.

Table 13: Eigen values of linear zed feedback system.

$$eig(A-B\cdot K) = \left\{0,\ -144,\ -30,-34,-9.2\cdot10^{-13},-0.13,\ -0.13,\ -0.13\right\}$$

5.8.2.4 Controller Tests

Two initial tests were run, one where the system was initialized with all three Euler angles to 0.4 radians and controlled so as to achieve zero conditions, the results can be seen in Figure 15. We see that after 600 [s] the maximum errors is on the ψ Euler angle, which for small angles is equivalent to ORF z axis, is 0.8594 degrees. We do notice that the ϑ and ψ axis still continue to oscillate. This could be to due gyroscopic effects due to the satellite being earth pointing, and the associated permanent rotations around the ORF y axis.

We notice the significant overshoot of the system, this is due to the fact that the magnetic torquers saturated to their maximum value of 0.0444; we note that for this simulation the saturation of the magnetic torquers was approximated with the hyperbolic tangent function. However, this controller is designed to operate close to the zero conditions, especially for the ϑ and ψ angles, so it is assumed that saturation will rarely be encountered. We also note that for the purpose of rejection of constant torques the gain was kept intentionally high.

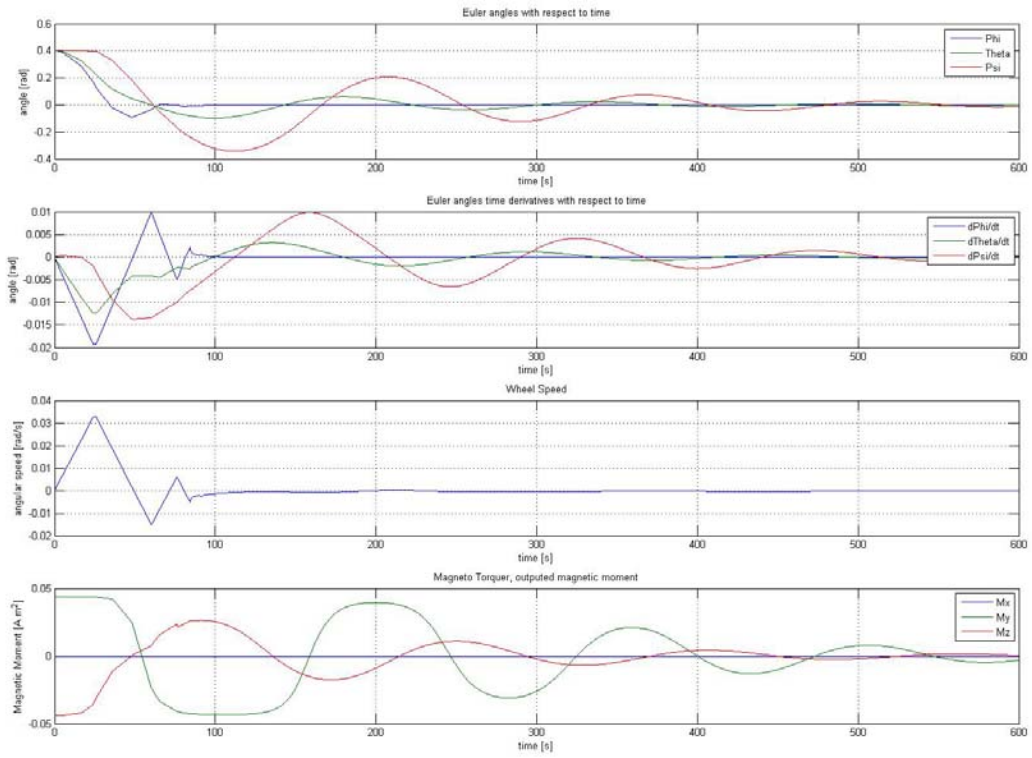

Figure 15: First test of controller

.

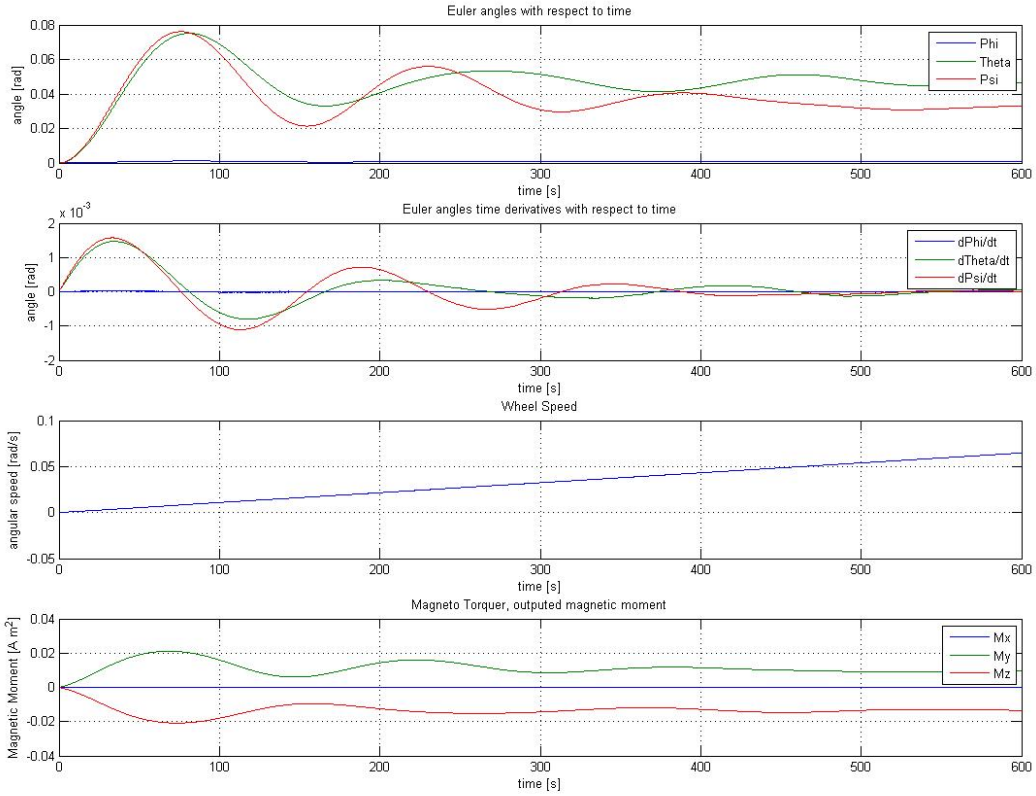

Figure 16: Second controller test

The second controller test involved applying a constant torque around all three axes equal to $4 \cdot 10^{-7}\, Nm$ with and an added random component with mean amplitude of about $6 \cdot 10^{-8}\, Nm$ the results can be found in Figure 16. Importantly we notice that the wheel maintains a constant acceleration in order to compensate the constant disturbance torque. If the wheel is not de-spinned it will eventually saturate.

Also of note is the small permanent error that on the ϑ and ψ angle; this is due to the lack of integrator term in the controller. The maximum constant error however is 0.003 degrees; however, this is in the case of the maximum expected disturbance torque. Considering the uncertainties on the attitude determination this value can be considered effectively zero. In fact the addition of an integrator will have no significant impact on the precision of the system while affecting the dynamics.

From the tests the controller it does shows good results along all three axes. Congruently it proves the viability of the model and the control strategy. However, we recall that this controller is only valid around a specific position along the Swisscube orbit attitude more study is needed in order to define the definite global control algorithms.

5.9 Dynamical Stability Analysis

5.9.1 Stability of the Constant Rotations

The system scanning discussed in § 5.1 foresees that the cubesat maintains a constant nadir oriented attitude. A direct consequence that the ORF is not an inertial reference system means that the stability of the constant rotation, since the satellite must continually point itself at the earth, must be analyzed.

Following a classical analysis as done by [Sidi 96-98] it is possible to analyze the effect of the inertia matrix on the rotational of the stability analysis:

Assuming a body in space with principal inertias (I_x, I_y, I_z) free in space with out any torques applied and we seek to find the stability analysis for a rotation around Z axis. Rewriting the Z term rotational speed terms as $\omega_z = \dot{n} + \dot{\varepsilon}$ where n is a constant term and ε is a small deviation from the constant speed. It follows that $\dot{\omega}_z = \dot{\varepsilon}$. Recalling the Euler moment equations:

$$\vec{M} = \dot{\vec{h}}_{BRF} + \omega \times \vec{h}_{BRF}$$

Where $\vec{M}$ is the external moment and $\vec{h}$ is the angular momentum. Setting the external moments to zero and imposing $\varepsilon \to 0$ the equations reduce to:

$$I_x \dot{\omega}_x + \omega_y n(I_z - I_y) = 0$$
$$I_y \dot{\omega}_y + \omega_x n(I_x - I_z) = 0$$
$$I_x \dot{\varepsilon} + \omega_x \omega_y (I_y - I_x) = 0$$

Combining the first equation with the second one can arrive to the following

$$\ddot{\omega}_x + n^2 \frac{(I_z - I_y)}{I_y} \frac{(I_z - I_x)}{I_x} \omega_x = 0$$

Equation 20

By taking the Laplace transform of Equation 20 it can be shown that Equation 20the will produce a non diverging solution only if the term $\frac{(I_z - I_y)}{I_y} \frac{(I_z - I_x)}{I_x}$ is positive. This implies that for the system to be stable:

$$I_z > I_x, I_y \vee I_z < I_x, I_y$$

This can be interpreted as to mean that if the body is rotating about the maximum or minimum moment of inertia then the rotation about that axis will be stable. This solution is only valid for bodies free from external torques and with constant rotational kinetic energy [Sidi, 97]. However, it is possible to find generalized results for axial symmetric spacecraft which also state that the rotation around the mayor inertia axis is stable. [Sidi, 100]

The fact that the satellite must always rotate around its mayor inertia axis has a direct impact on the configuration of the satellite. Recalling that the payload must point from 17 degree to 29 degree downward from the ORF y axis, this could also be seen as a rotation about the ORF x axis, see

Figure 17 . We also recall that with respect to the earth the ORF is rotating with a constant angular speed of $\omega_{ORF} = \frac{-2\pi}{P}\hat{y}_{ORF}$, where P is the orbit period in seconds.

Taking into account that: there is constant rotation around the ORF y axis, that the payload is solidary to the SRF –y axis, and that the SRF –y axis must be rotated 17 to 29 degree downward, the only possible solution is to **rotate the principal inertia matrix direction in order to assure that the mayor inertia axis is as parallel as possible to the ORF y direction.** Following this results a concentrated effort was made in cooperation with the configuration team to optimize the inertial properties of the Swisscube by achieving an principal inertia matrix congruent with the rotation. Following the last iteration of the configuration of the Swisscube internal structure the Swisscube principal inertia matrix was very close to desired results, the current rotation values are expressed in Table 14. We note that we seek $R_y = R_z = 0$ and $R_X = 17 to 25$ degrees.

Table 14: Swisscube principal inertia matrix rotation angles from SRF

Direction	Rotation
R_x	14.8
R_y	-1.3
R_z	6

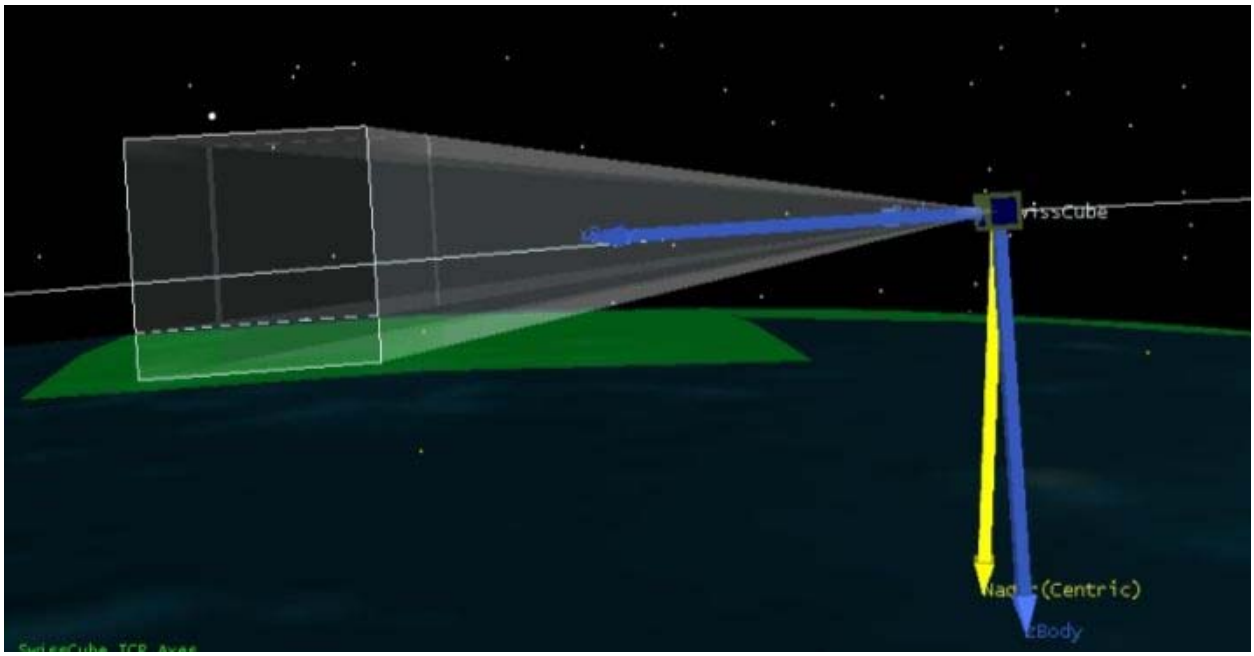

Figure 17: Shows the 17 to 29 degree rotation that the SRF frame must have around the x axis with respect to the ORF in order to scan the atmosphere limb [Scheidegger].

5.9.2 System Vibration Modes (AF)

Since the Swisscube Cubesat makes use of two flex antennas they contribution to the general system dynamics are taken into account. The current specification foresees two beryllium copper antennas

whose properties are summarized in Table 15, the antennas are assumed to have a rectangular cross-section, the geometric configuration can be found in Appendix B.

The main concern to the ACDS subsystem are the possible low frequency vibration modes of the flexible structure since a possible excitation of an non-symmetrical mode's resonance with an external disturbance would create unstable variations of the spacecraft attitude [Wertz, 551].

An initial analysis was done by modeling just the first vibration mode of both antennas. The Monopole antenna however is in a more critical configuration. We modeled the system initially as a free bar connected to a fixed wall at one end and free on the other. At this point we model an equivalent mass spring system with the values $m_e = 0.243M$ and $k_e = \frac{3EI}{l^3}$ [Splinner, 68]. We note that this model is note entirely accurate and may require a more a more rigorous study in order to confirm the results [Wertz, 549].

These were used though to give initial approximations of the resonance frequencies as $w_0 = \sqrt{\frac{k_e}{w_e}}$.

Using an equivalent procedure for the dipole antenna we find both natural frequencies these are tabulated in Table 15: Physical Properties of the flex antennas.

Table 15: Physical Properties of the flex antennas

	Length [m]	Mass [g]	Moment of Inertia, rectangular cross-section [m^4]	Approximate natural frequency of first vibration mode [s^{-1}]
Dipole Antenna	0.348	3.71	9 e-012	25
Monopole Antenna	0.610	7.17	9 e-012	0.0028

Of the disturbances forces the most significant ones are the gravity gradient and the residual magnetic dipole force. Since the attitude is nadir oriented it is possible in normal operating conditions we assume the gravity gradient as null or constant, it therefore does not significantly affect the vibration dynamics.

The residual magnetic dipole however, depends on the magnetic field. A very simple approximation of the magnetic field can be made in the ORF by considering the magnetic field components as $B_x = B_0 \cos(\alpha), B_y = 0, Bz = 2B_0 \sin(\alpha)$ where α is the latitude and B_0 is the field strength at the equator [Courtois et al, 484]. Therefore, the excitation frequency $\dot{\alpha}$ is directly related to the orbit speed and consequently the altitude, tracing $\dot{\alpha}$ for different altitudes we see the range of frequencies that are excited by the residual magnetic dipoles. For circular orbits the orbital frequency is $w_{0R} = \left(\mu r^{-3}\right)^{1/2}$ with μ the earth's gravitational constant [Larson et al, 137]; In Figure 18 the harmonic response of the monopole antenna as well as the range of frequencies due to magnetic excitations can be seen.

In fact we see that at the lowest possible altitude 400 [km] the orbital frequency is 0.0011 which is around 40% of the first natural frequency; since all further modes will have faster frequencies than the first one we can safely ignore all higher vibration modes.

While the initial analysis shows that the antennas will have a frequency higher than the magnetic field excitation this is not the only harmonic excitation possible; in addition the relatively low natural frequency of the antenna raises the possibility of interaction with other system vibrations.

In addition, apart from the magnetic field, It is certain that some of the frequencies dynamics will excite the antenna resonance frequency. Taking for example an approximation of the bandwidth of the control system as defined by [Larson et al, 379]: $\omega_n = \sqrt{\frac{K_p}{I}}$ where $K_p \geq \frac{T_d}{\theta_e}$ and T_d is the disturbance torques while ϑ_d is the maximum allowable motion. We set $K_p = \frac{2T_d}{\theta_e}$ since the actuators are dimensioned for twice the possible disturbances. Taking $I = 2 \cdot 10^{-3} [kg\, m^2]$ as a typical inertia we calculate a natural frequency of $\omega_n = 0.09\,\text{rad/s}$ which is significantly higher than the system frequencies. This guarantees that there will be a non-negligible component of the system vibrations which will excite the system.

Further studies into this phenomenon are advisable in order to better quantify the ACDS system loads.

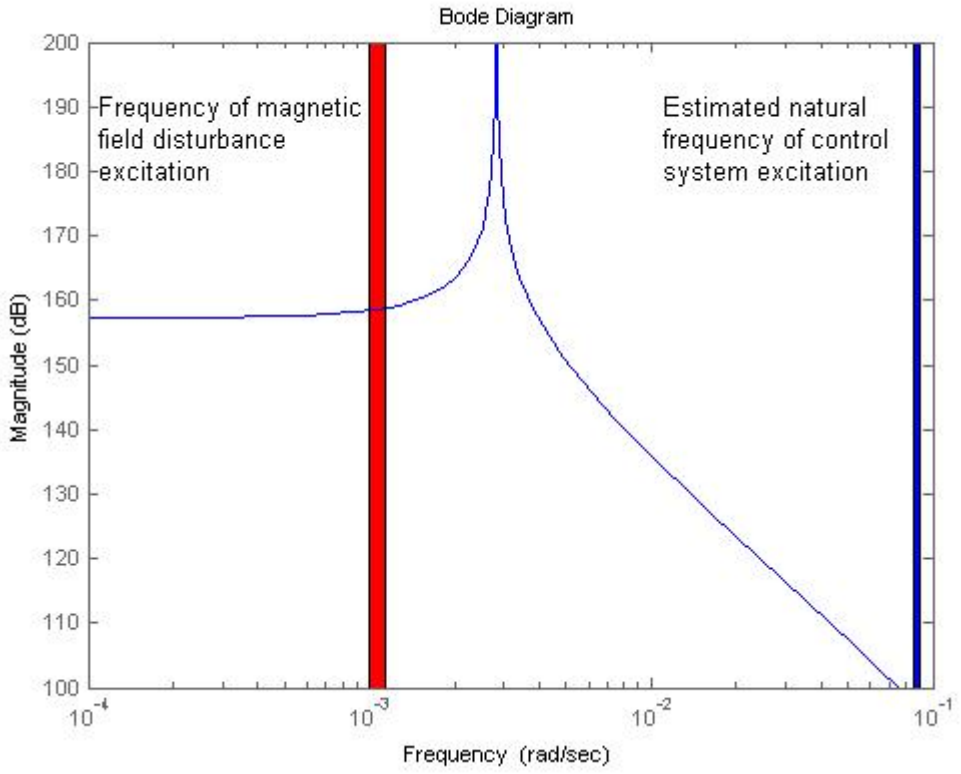

Figure 18 : Frequency response of monopole antenna with frequency range of magnetic disturbances and system excitation

5.10 Sensors Simulations

Simulink models of the magnetometers and the solar panels were created, in order to test these sensors behavior. Another reason for doing these simulations is to find out what steps need to be taken in order to retrieve the attitude, which will be helpful when the time of implementation of the real system has come. Finally, in future work, if these sensors models are combined with the estimation algorithm (which is not yet in the Simulink format), and even with the controller and dynamic model, a simulation of the whole system behavior during an orbit will be possible.

5.10.1 Magnetometers

The inputs needed to find the magnetic field direction are the magnetometers outputs, the magnetotorquers inputs and the Earth's magnetic field model. Parameters such as the distance between the magnetic sensors and actuators, the number of coils of the actuators and the orbit are considered known. The steps needed to be done in order to find the magnetic field vector are summarized in the following flow diagram (Figure 19).

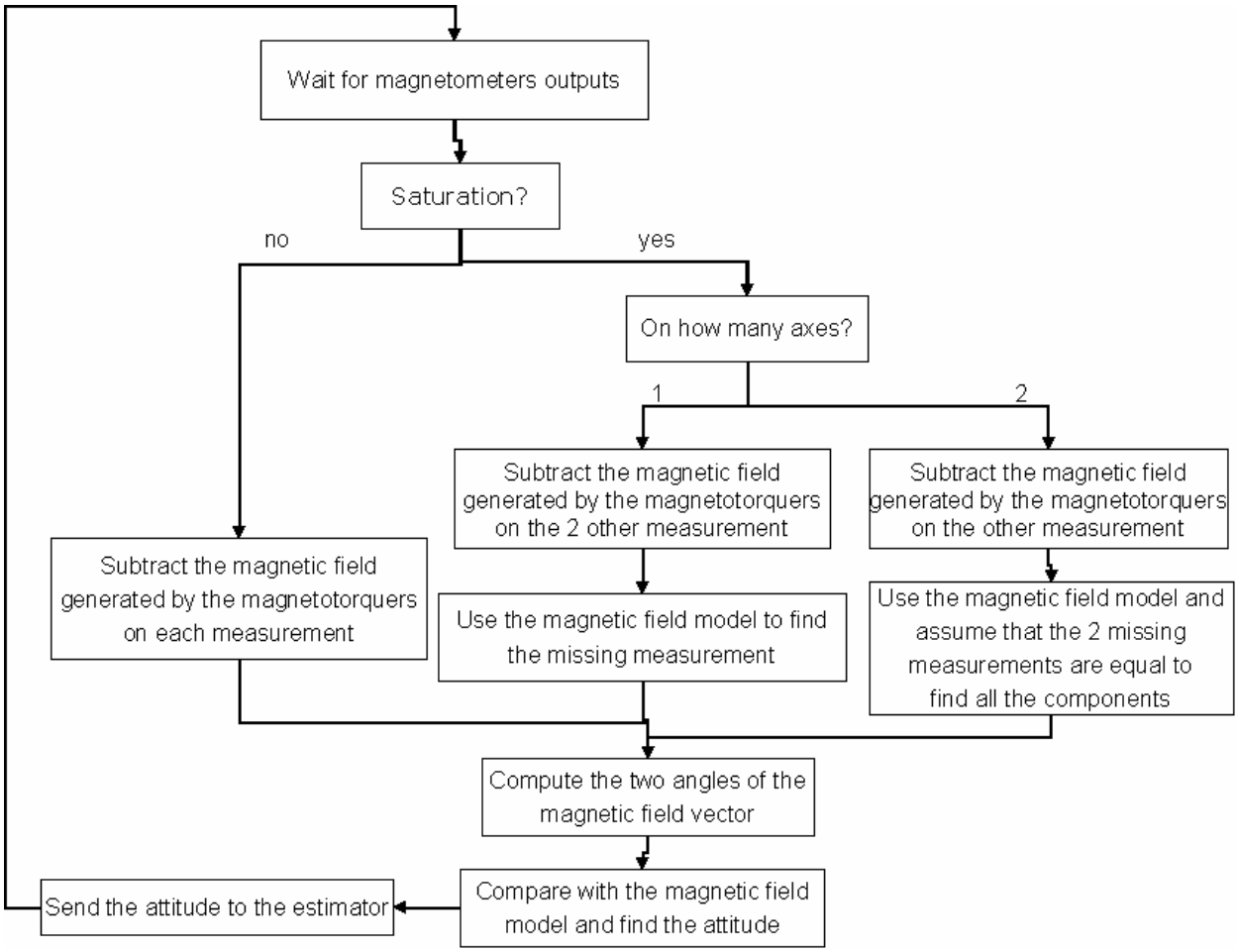

Figure 19: Flow diagram of the steps to retrieve the attitude using the magnetometers

As explained in section 5.4.2, saturation can occur on one or two magnetometer measurements, but the magnetic field can still be retrieved accurately. The magnetic field model only needs to inform

about the expected field strength, and the saturated component(s) can be found using the unsaturated component(s). If there is one saturated measurement, the calculation is straightforward, and if two measurements are saturated, constraining them as being equal allows the vector to be found also. Nevertheless, in the latter case, the estimation of the vector becomes less accurate, and the measurement noise covariance can be changed in the extended Kalman filter algorithm in order to take that into account (more explanation about the extended Kalman filter will be provided in section 5.12).

When all three components of the vector are known, the two angles defining it can be computed. The final step to retrieve the attitude from the magnetometers is to compare the computed magnetic field vector with the magnetic field vector given by the model, in the orbital reference frame (when all the angles are zero). Then, the rotation angles that allow the theoretical vector to be rotated to the measured vector, which are the attitude angles, can be found. The attitude being retrieved, these data can be used by the estimation algorithm to find the best prediction of the attitude, and the whole operation can be repeated.

A Simulink model that can be used to simulate part of the aforementioned process was created (Figure 20). The magnetic field model, which is also used for the controller simulations, takes as inputs the Tait-Bryan angles defining the attitude of the satellite, and returns the magnetic field strengths along the three axes. The magnetic field is computed by interpolating values of a list of magnetic field strength around the Earth, which can be found on the NASA website. The magnetic field model changes its outputs in function of the simulation time, which is in relation with the orbit position.

The magnetic field along an axis is not only created by the Earth, and this is why the fields created by the magnetotorquers are added, along with some noise. It was assumed here that one magnetotorquer only influence the field along the axis of its coils, but it is not really true, as the perpendicular component of the field can be non-negligible at certain positions. Thus, once the dispositions of the magnetotorquers and magnetometers are known, the contributions of the three actuators along any axis should be computed.

After the noise being reduced with a low-pass filter (which can either be implemented on analog circuits or in the software), the sensors are modeled by a quantizer, representing the resolution, and a saturation. The components magnetic field vector can then be calculated by subtracting the measured value by the contributions of the magnetotorquers. The angles defining the vector (in polar coordinates) can then be found, and compared to the vector of the case where the Tait-Bryan angles are all set at zero to find the attitude.

In the Simulink model, the part where the rotation matrix between the two vectors is calculated is not written yet. The model takes into account the 2D case, where one angle of the magnetic field vector is computed. The remaining part that needs to be done includes a copy of what was done here but for another pair of axes, and above all the rotation matrix that compares the two 3D vectors. Indeed, in the 2D case, a simple subtraction is the only operation needed to find the rotation of a vector, but more complicated operations are needed for the 3D case. If this model is to be included in a bigger simulation that takes into account the whole satellite with the controller and the dynamics, the attitude angle inputs of this model can be substituted by the outputs of the estimation system, and the magnetotorquers inputs information can be received by the control part.

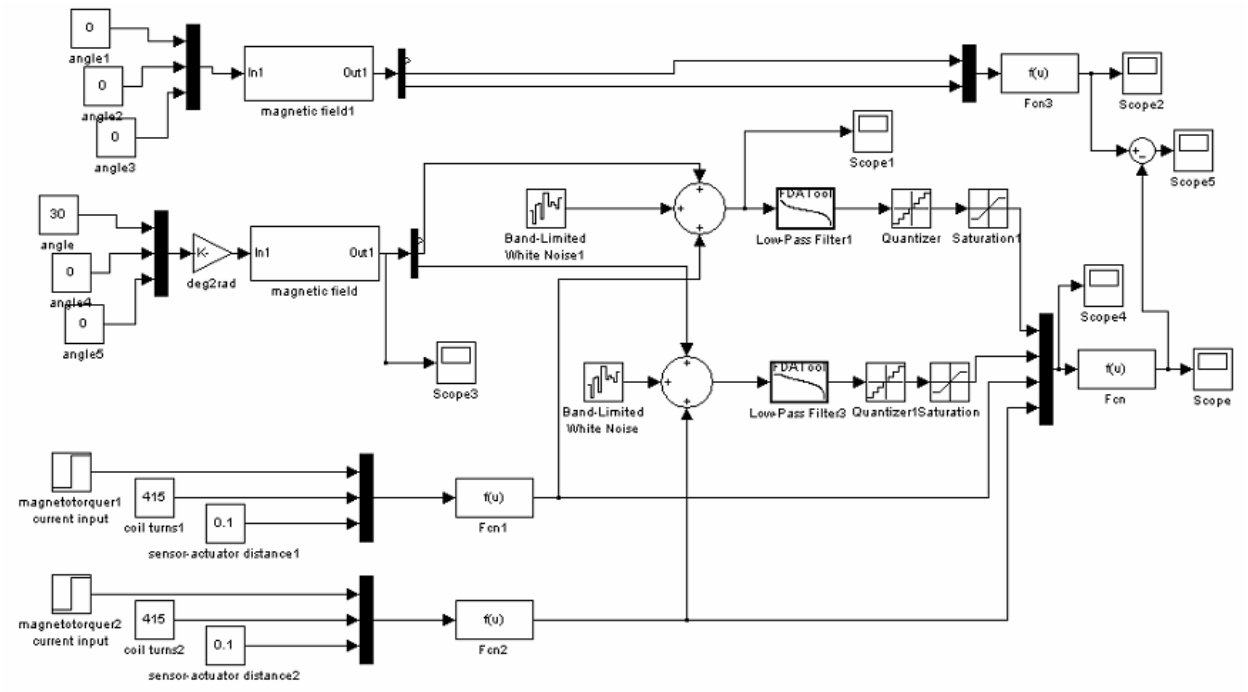

Figure 20: Simulink model of the magnetometers attitude retrieval

An example of the output of the simulation is shown below (Figure 21). The initial conditions are that the satellite Tait-Bryan attitude is (30, 0, 0) degrees and that all the magnetotorquers are turned off. One angle of the attitude is computed by comparing one angle of the measured magnetic field vector with the one of the "zero attitude angles" theoretical vector. The non-immediate rise time is due to the low-pass filter. At time t=5, a magnetotorquer was activated and the compensation can be seen, with the settling time also due to the low-pass filter, which saw a sudden change in its input. The attitude angle is correctly estimated, with an accuracy of below 5 degrees, except during the settling time due to the filter.

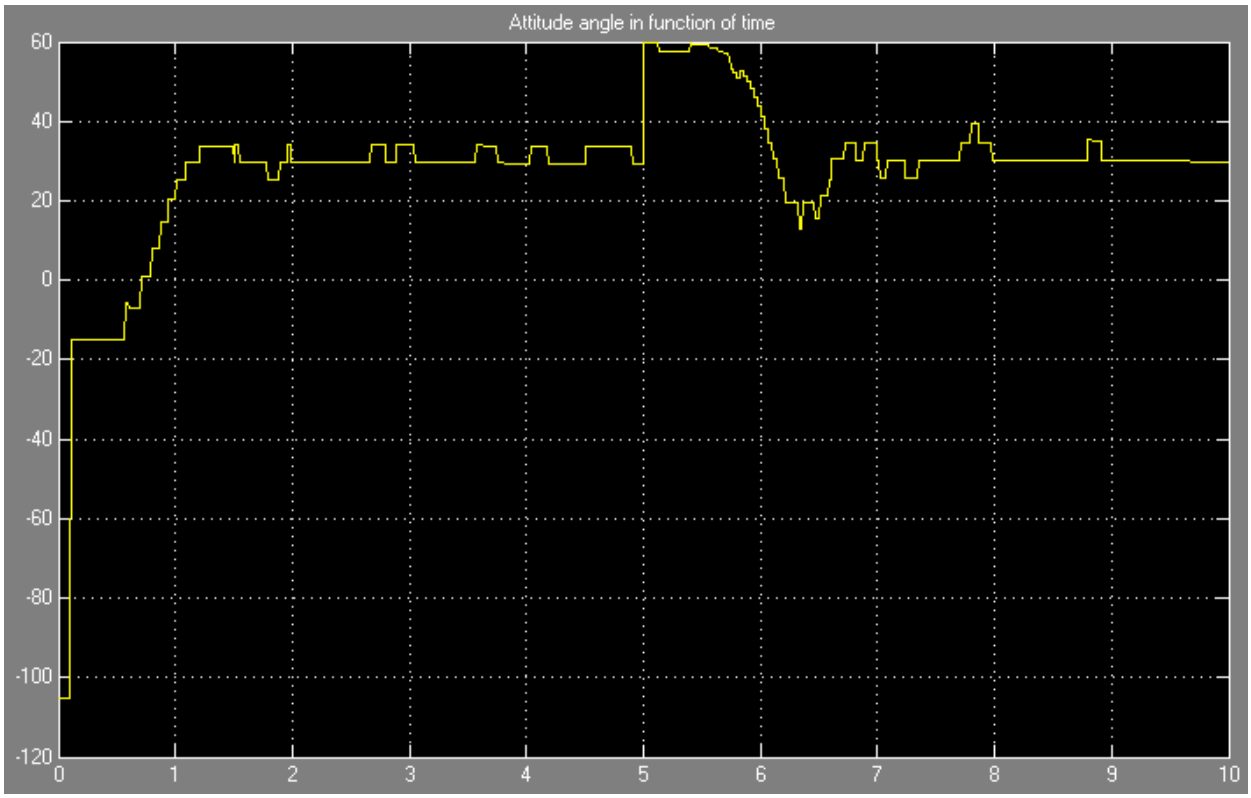

Figure 21: Output of an estimated angle using magnetometers in function of time. A magnetotorquer was actuated from time t=5.

5.10.2 Solar panels

The solar panels can be used as sun sensors by calculating for each panel the angle of incidence of the sun rays, knowing the power output of each panel. To do so, the maximal power output, when the sun is at the vertical of one panel, has to be known. The major unreliability of this sensor system lies here, because after degradation, the maximal power output will be reduced and the estimation will be off by a certain angle.

The inputs of this estimation system, which are the power outputs of the panels, will come from the Electrical Power Subsystem, which would still have to monitor these outputs even if the solar panels are not used as sun sensors. This means that very few devices are needed for the use of these sensors. The variation of the power output of one panel with respect to the angle of incidence is supposed to follow a cosine law, but if it is not the case, a different law can be implemented in the program after identifying it experimentally. In the model, $P = P_{\max} \cos(\alpha)$, P being the power output, $P_{\max}$ the maximal power output and α the incidence angle of the sun light.

The inputs of the simulation (Figure 22) are the maximal power output and the two polar angles defining the sun vector. A model of the sun vector has not been created yet, but it is quite easy to do, because of the sun-synchronous orbit of the Swisscube: indeed, the sun direction will be a function of the cosine of the angle between the orbit and the Earth-Sun vector.

From the direction of the sun, the power outputs of all five panels are simulated using the cosine law, and assuming a cutoff angle of 20 degrees below which no output is produced, following the advice of other Cubesat group researchers. Noise is added to these measurements, and low-pass

filters are included to counteract it. Finally, the angle of incidence on each panel is calculated using the cosine law.

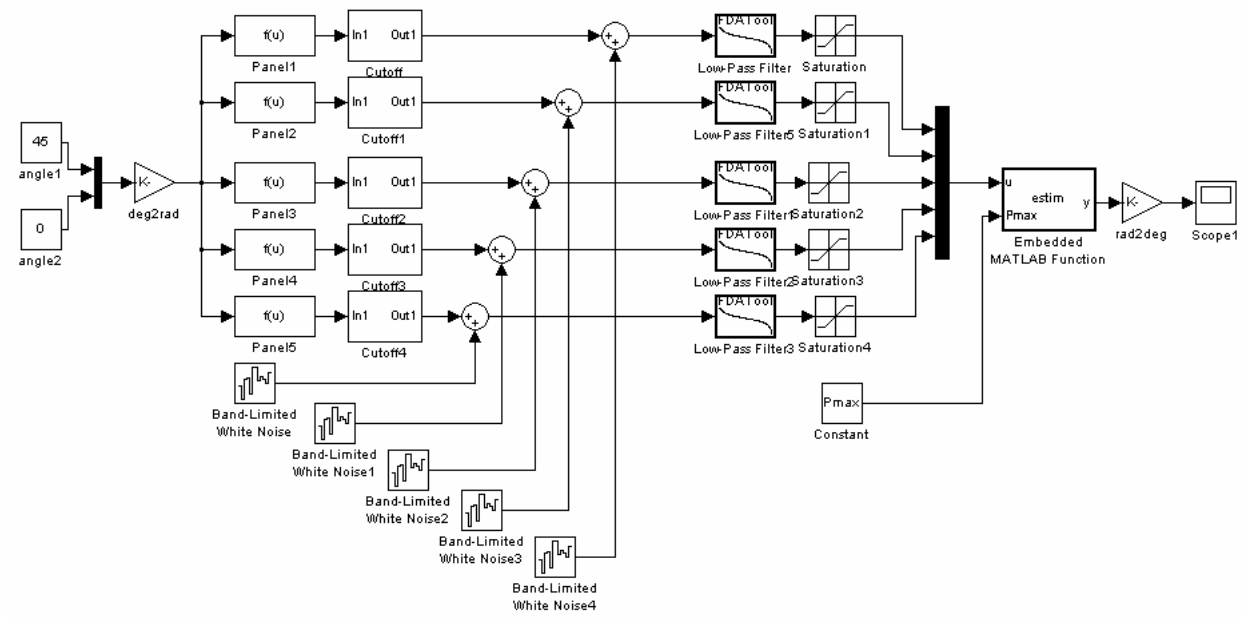

Figure 22: Simulink model of the solar panels used as solar sensors

The sun vector is not computed, as there is redundant information about it. However, it does not necessarily need to be found, as the scalar power outputs of the panels can be readily used in the Kalman filter [Humphreys]. The angle of incidence calculation block is hence not needed if a Kalman filter is used, and no cosine needs to be computed, which is good in a computational resource point of view. In [Humphreys], each solar panel by itself gives information about the attitude of the satellite, and the non-necessity of the sun vector retrieval reflects that, as only one solar panel output should be able to improve the estimation, even if it is impossible to know the sun vector with only one output.

Simulating with a noise that has 1% amplitude of the maximal power output, the angle accuracy is around 5 degrees. This value will be used afterwards for the extended Kalman filter simulations. More complete specifications of the solar panels will allow a better identification of their accuracy.

5.11 Observability

A dynamic system is called observable if each one of its states can be uniquely determined from its inputs and outputs, given its model. The issue of observability is very important, as it provides information about the number and type of sensors needed in order to determine the system states, as unknown states pose problems to control the system. For example, if the satellite is observable with sensors that only give information about the angular position, and not about the angular velocity, then rate gyros may not be needed. Nevertheless, the observability concept does not give any information about the accuracy of the states estimation, as it only takes into account the model. The differences between the model and the actual system, which cause different states evolutions between the theory and the real system, are overlooked. This explains that further studies and simulations have to be done after the system is proved to be observable to investigate these more practical issues.

5.11.1 Observability of a linear system

Adopting the notation from [Grewal et al.], the continuous-time state-space representation of a linear time-invariant system is:

$$\dot{x}(t) = \phi x(t) + Cu(t)$$
$$z(t) = Hx(t) + Du(t)$$

where z are the measurements, x the states and u the inputs.

Although the Swisscube model is nonlinear, this representation fits well to the liner Kalman filter, which will be presented later. Furthermore, the analysis done up to now often involves the model linearized at a functioning point.

If the measurement sensitivity matrix H is invertible at any time, then the system states can be uniquely determined as $x(t) = H^{-1}z(t)$. In this case, the model is called completely observable. However, in the general case, H is not invertible, as that would mean that each state has to be measured, which is not desirable because of the related issues of the corresponding sensors implementation. Each state does not need to be measured for the system to be observable, as it can still be observable over a time interval, some states being linked to each other by the mean of differential equations. Estimation theory provides algorithms that allow the determination of the states that are not measured, as long as the system is observable.

From linear system theory, a system is observable if:

$$Rank(Q) = Rank\begin{bmatrix} H \\ H\phi \\ H\phi^2 \\ \vdots \\ H\phi^{n-1} \end{bmatrix} = n$$

where Q is the observability matrix, and n the number of states of the system.

5.11.2 Observability of the Swisscube

For different functioning point, the nonlinear model of the Swisscube was linearized (calculating the Jacobian at the different points) and the observability tested. It was found out that the system is always observable with only two angular position outputs (with only two angular positions being measured) except for the singularity when the ψ angle is $\pi/2$. This means that having information about the angular around two axes, such as with a pair of 2D magnetometers, is enough to predict the system attitude and attitude rate using the model, but as it will be shown below, an open-loop prediction can be highly incorrect with 10% of modeling error. Nevertheless, the fact that the system is observable with two angular position measurements is important, because this situation happens during eclipses if sun sensors and magnetometers are chosen. If the system was not observable in such a case, the attitude prediction could be lost.

A more complete analysis of the observability of a nonlinear system can be done by applying nonlinear systems theory, using Lie brackets. This was not done here, but it can be applied with a quaternion model, which should be exempt of singularities.

5.12 Attitude determination algorithm

In order to link the information of the sensors to an estimation of the attitude, an algorithm has to be used. It is possible to use only one sensor outputs and have a Leuenberger-type estimator (which does not take into account the sensors accuracy and redundant information), but one can sense that the remaining sensors could be considered for a better estimation. The goal is to use the fact that redundant information is available and improve the accuracy of the prediction by giving different importance to the sensors that are not as accurate as each other. Indeed, each sensor, however inaccurate its output is, should increase the overall estimation of a state, as it still gives additional data. In 1960, R.E Kalman published a paper describing a recursive solution to the discrete-data linear filtering problem, and the resulting tool, the Kalman filter, can be used to estimate the states of a system in a way that minimizes the mean of the squared error and can thus be described as an optimal filter. It is used to estimate the states of a linear process, but, thanks to the extensive research done on this subject, an improved version, the extended Kalman filter (EKF), can be applied on non-linear processes.

There are also other methods, such as a model-free Kalman filter and a deterministic approach (q-method for the Wahba's problem), which can be used with a quaternion-represented model. The former converges faster than the extended Kalman filter, but can "lose" the three-axis attitude estimation when two non-collinear vector observations are not available, such as during eclipses if only sun sensors and magnetometers are used. There is the same problem with the q-method, which also needs at least two non-collinear measurements, as it computes the rotation matrix between the two vectors and provides a point-to-point solution without relying on its precedent results. Hence, these methods have not been implemented or tested for the Swisscube.

In this section, an attitude determination system based on the extended Kalman filter is presented and discussed. Indeed, this approach seems to be the better one, as the model is used, and it was also considered for other satellites with the same sensor configuration as the Swisscube (SSETI-Express). During eclipses, it has been shown that it is possible to obtain a correct three-axis attitude estimation with only the magnetometers data by using an EKF [Psiaki et al.]. Nevertheless, as it will be shown below, the corresponding accuracy of the estimation lowers significantly. Because of the linearization of the model, convergence is not guaranteed if the estimation error is too large, and simulations allow us to test the limits of the algorithm. Before these results are shown, some theory about the Kalman filter and its versions for nonlinear systems will be discussed and presented.

5.12.1 Extended Kalman Filter Theory

The Kalman filter is a linear estimator that takes into account the noise in the system and in the measurements, assumed to be Gaussian with zero-mean. The prediction of the states is a linear combination between the open-loop model-based prediction and the difference between the predicted outputs and the measured outputs, called innovation (see Figure 23). The Kalman gain, which is a matrix that changes over time depending on the error covariance, multiplies the innovation and put more or less importance on the measurements, in an optimal way.

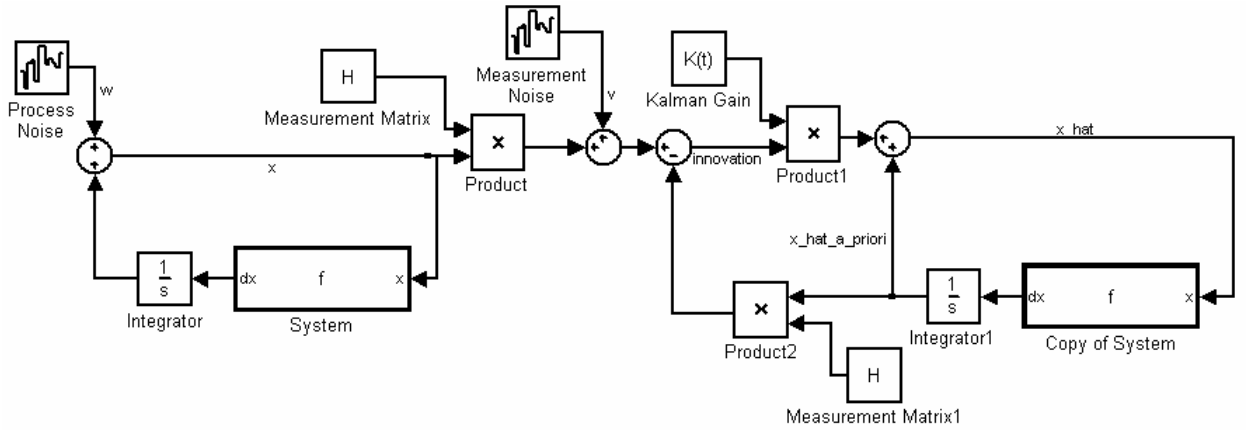

Figure 23: Block diagram of the dynamic system and the Kalman filter

The Kalman filter is supposed to estimate linear systems states, but as for the control of nonlinear systems, there exist different solutions for nonlinear systems to be considered using linear system tools. For example, the linearized Kalman filter and the extended Kalman filter are two approaches for nonlinear problems. The linearized Kalman filter precomputes the matrices H, K and Φ offline around a trajectory and is therefore efficient for real-time applications, but also less robust than the extended Kalman filter, which computes these matrices at each time step around the current state estimates. Indeed, the farther from the trajectory the system is, the more effects the higher-order terms will have, and linearizing around the previous point insures that the distance between the linearization point and the system states is minimized, given that the sampling rate is high enough.

The many kind of Kalman filters exist in both continuous and discrete versions, with slightly different Kalman gain equations. Here are the main equations for the continuous extended Kalman filter:

Nonlinear dynamic model:

$$\dot{x}(t) = f(x(t),t) + G(t)w(t)$$
$$z(t) = h(x(t),t) + v(t)$$

State estimation and predicted measurement:

$$\hat{\dot{x}}(t) = f(\hat{x}(t),t) + \overline{K}(t)[z(t) - \hat{z}(t)]$$
$$\hat{z}(t) = h(\hat{x}(t),t)$$

Linear approximation:

$$F(t) = \left.\frac{\partial f(x(t),t)}{\partial x}\right|_{x=\hat{x}(t)}$$

$$H(t) = \left.\frac{\partial h(x(t),t)}{\partial x}\right|_{x=\hat{x}(t)}$$

Kalman gain equations:

$$\dot{P}(t) = F(t)P(t) + P(t)F^T(t) + G(t)Q(t)G^T(t) - \overline{K}(t)R(t)\overline{K}^T(t)$$
$$\overline{K}(t) = P(t)H^T(t)R^{-1}(t)$$

v(t) and w(t) are respectively the measurement and the process noises, and it is assumed that they are Gaussian, white and with a covariance of R(t) and Q(t), i.e. $v(t) \sim N(0, R(t))$ and $w(t) \sim N(0, Q(t))$. P(t) is the covariance matrix of state estimation uncertainty and $\overline{K}(t)$ is the Kalman gain.

In these equations, we can notice that the $\overline{K}(t)$ will be bigger if R(t) is smaller. This means that more importance will be given to the measurements if they are more accurate, which is a desirable behavior for the estimator. The assumptions that the noise is white can be false when there is a bias, and it can be essential to model these parameters for the estimator to converge. For instance, the Swisscube will be subject to disturbances, but most of them will be constantly acting along one direction, such as the aerodynamic drag, and considering them as white Gaussian noise can in the best case slower the convergence of the EKF, or in the worst case cause the estimation to diverge. However, these disturbances are easy to model, and including them in the EKF equations is not a difficulty.

5.12.2 Extended Kalman Filter Simulations

Simulations of a continuous EKF were done in MATLAB, applying the equations shown above. The model was the one with no wheel, because of some simulation problems, and the inputs are set to zero. The behavior of the system with a given initial condition, and the estimation of the states given an initial error between the estimated states and the "real" states are the outputs of the simulations.

A difference of 10% between the model and the real system is assumed: for instance, the moment of inertias, mass and position of the center of gravity are 10% larger or smaller in the real system. What interests us is whether the estimation converges to the real system states or not, despite these model errors. If it converges, the interesting information is the speed at which it converges, and the accuracy of the estimation, which is the approximate range between which the estimation stays around the correct value.

In the simulations, the sensors that are supposed to be used are the magnetometers and the solar panels. The sensors models are not included, and the sensors here are only supposed to return the value of the attitude states. In other words, the conversion between the sensors measurements and their attitude estimation are omitted here. The sun and magnetic field vectors are initialized at the beginning of the simulation, and their attitude estimations directly come from there.

It was observed that when the difference between the initial error between the EKF and the real system was too big, around 50 degrees for the angles, the EKF does not converge to the desired value. A solution to this problem is to set the initial conditions of the EKF as the angle that can be estimated with the sensors alone, without the model, like it is done with a model-free Kalman filter. In other words, the initial conditions of the estimation can be set as a weighted average of the estimations of each sensor, and this will ensure that the estimation does not diverge, as the difference between the real system and the initial estimation will be a lot less than 50 degrees, thanks to the accuracy in the order of the degree of the sensors. It is also a good idea to implement in the final system a fault-detector in the software in case the estimation diverges, especially after eclipses. It can be done by comparing every few minutes the estimation of the EKF with the estimation of

the sensors alone, and if the difference is too big, to set the EKF angle states to the one returned by the sensors.

Different initial conditions of the error were tested to see the range of convergence of the estimation. Two cases were taken into account: the no-eclipse case, where both the sun sensor and the magnetometers data are available, and the eclipse case, where the sun is not in the view of the satellite.

5.12.2.1 No-eclipse case

The following simulation was done with an initial error between the real system and the EKF estimation of respectively 30 degrees and 20 degrees/sec for the attitude angular positions and the attitude angular velocity. The sun and magnetic field vectors were defined to be perpendicular to each other, meaning that all angular positions are measured, with redundant information about at least one of them.

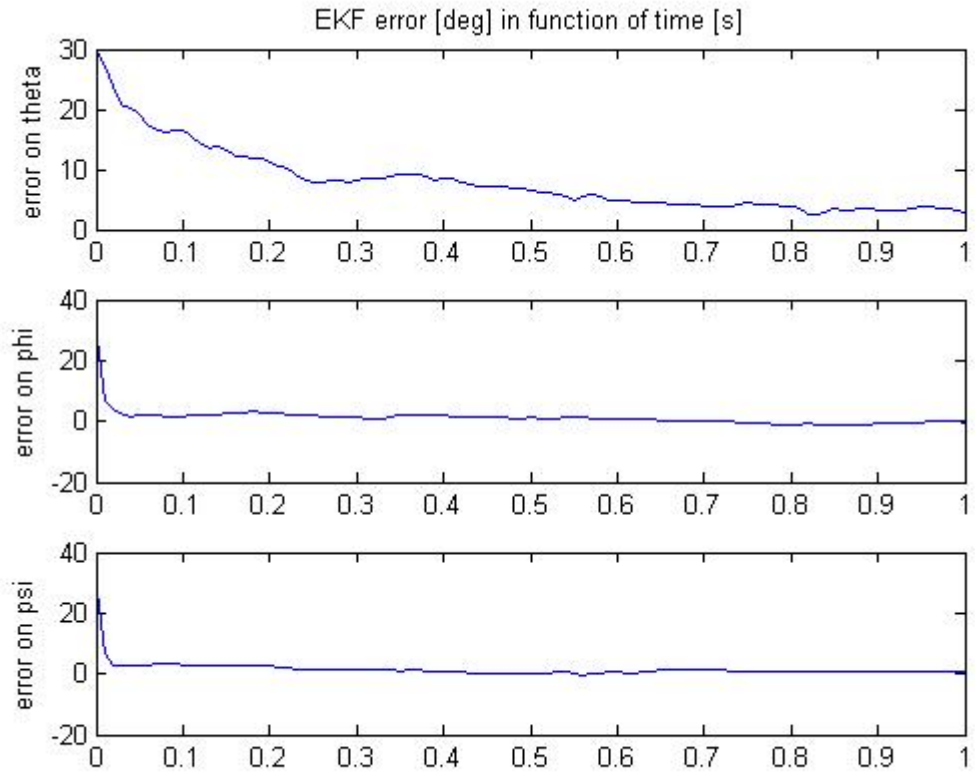

Figure 24: Errors on the attitude state estimates in function of time

The angles estimation error converges quickly to zero for the two last angles (see Figure 24). For the first one, the convergence is slower, with a remaining error of 3 degrees after one second.

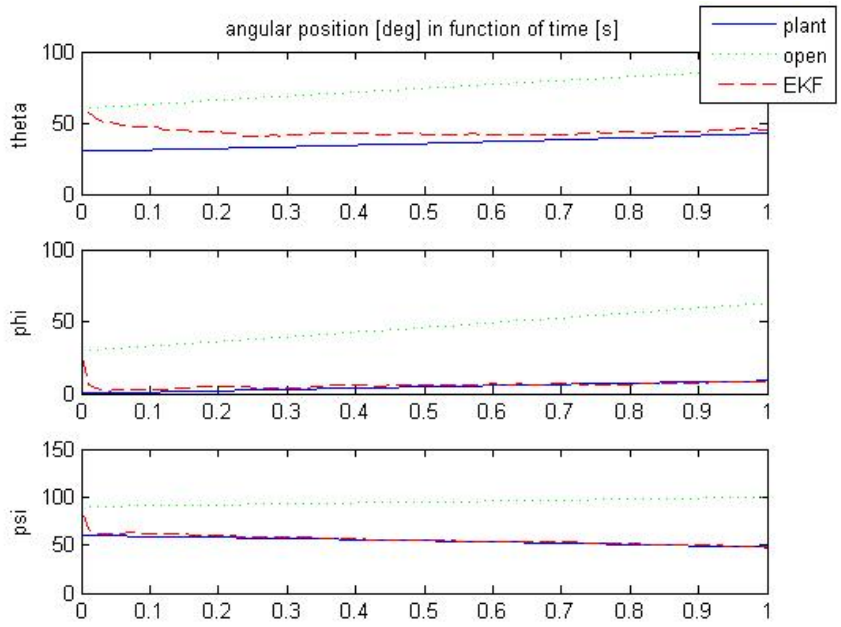

Figure 25: Evolution of the angular positions of the real system and the angular positions estimates of the EKF prediction and of the open-loop prediction

There is a big difference between the real system behavior and the model behavior (see Figure 25), because of the modeling error that were included, and also because of the different initial conditions. The EKF angle estimation quickly converges to the real system angle when measurements of all three angles are available via the sun and magnetic sensors.

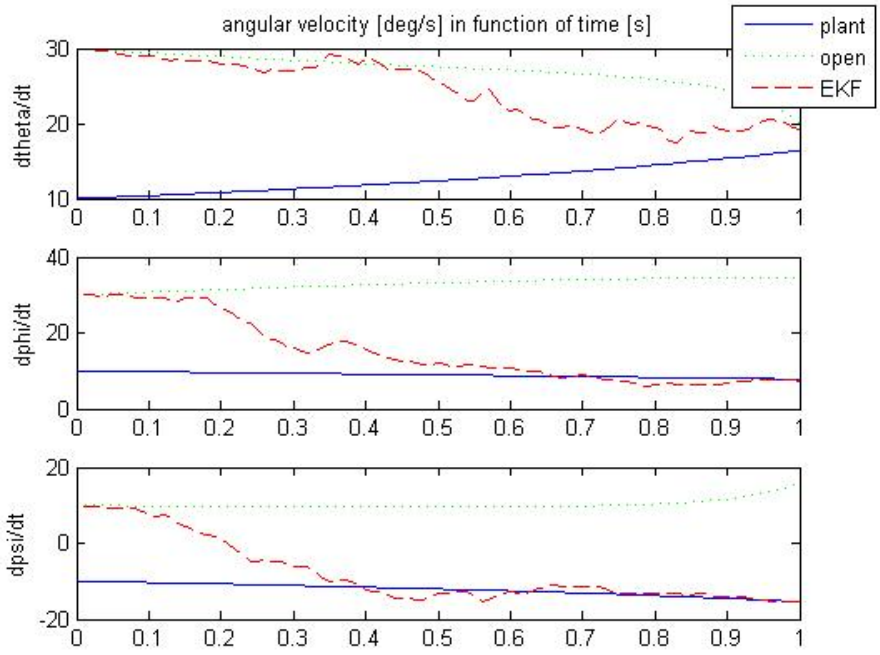

Figure 26: Evolution of the angular velocities of the real system and the angular velocities estimates of the EKF prediction and of the open-loop prediction

The derivatives of these angles, or angular velocities, are not measured, but the estimations also converge, because they are retrieved via the model, and if the angles are correctly estimated, so are their derivatives after a certain time (see Figure 26), the system being observable.

If the error is of 5 degrees and 5 degrees/sec, the estimation stays under a 4-degree range for the first angle and under a 2-degree range for the other ones, as shown in the following simulation results (see Figure 27, Figure 28 and Figure 29). The same increase in accuracy and stability can be observed for the rates of the angles. Thus, from a 30 degree error, the EKF is capable of converging to the right value at around 3 degrees around it.

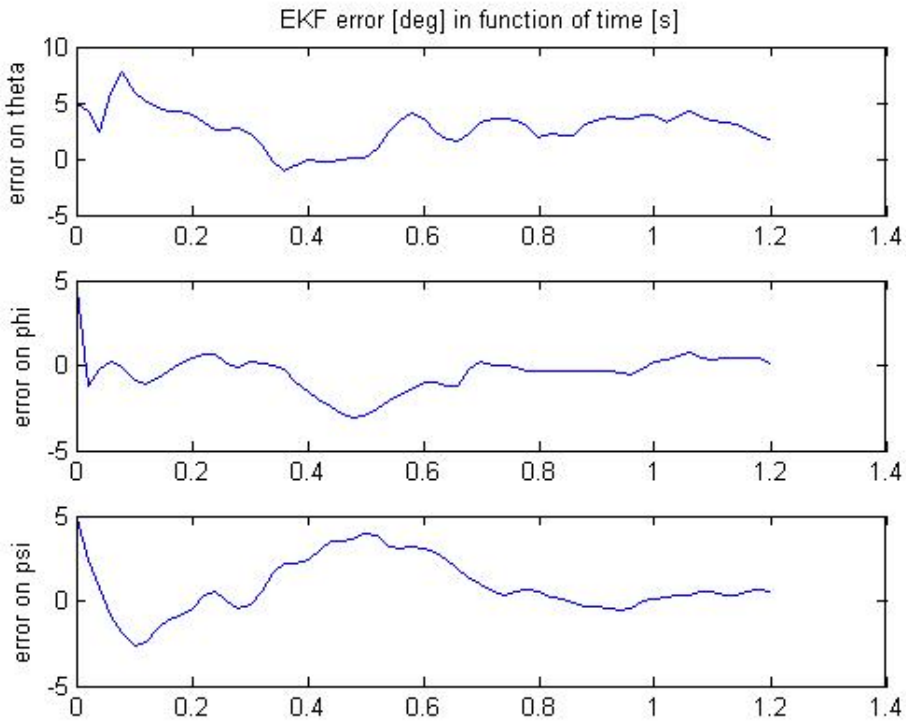

Figure 27: Errors on the attitude state estimates in function of time with an initial error of 5 degrees

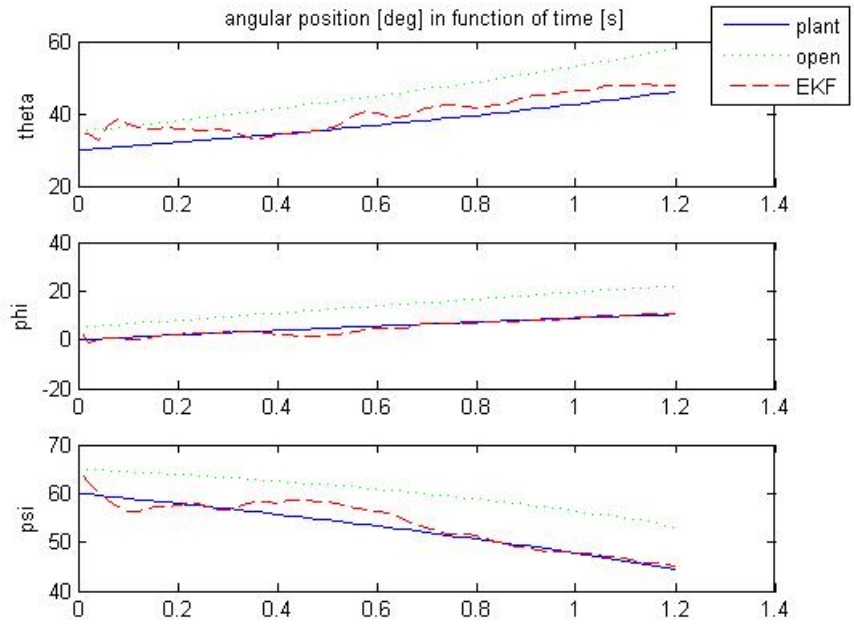

Figure 28: Evolution of the angular positions of the real system and the angular positions estimates of the EKF prediction and of the open-loop prediction, with an initial error of 5 degrees

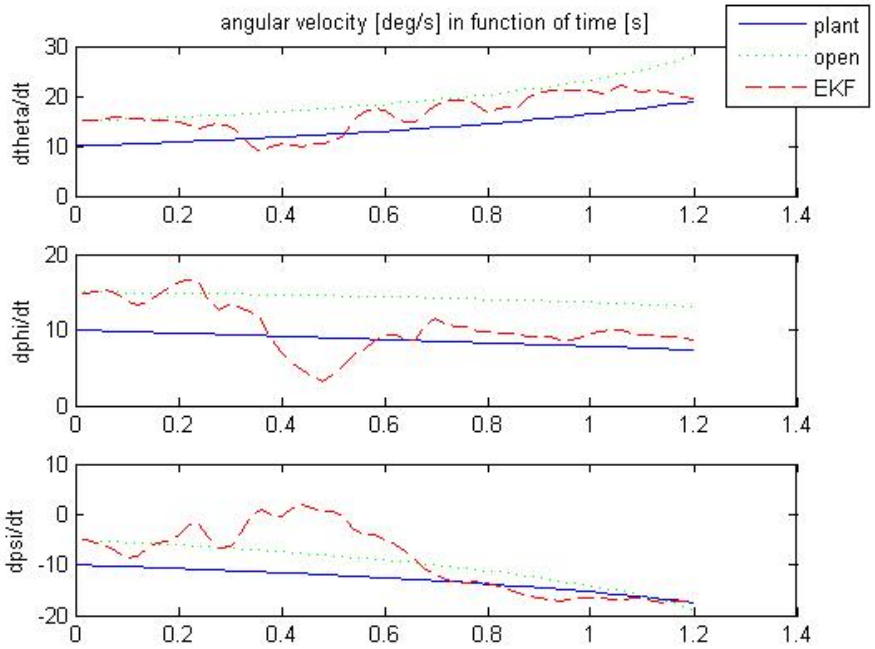

Figure 29: Evolution of the angular velocities of the real system and the angular velocities estimates of the EKF prediction and of the open-loop prediction, with an initial error of 5 degrees/sec

5.12.2.2 Eclipse case

If there is an eclipse, the estimation is less accurate, because of the loss of information. In fact, if one face of the cube is perpendicular to the magnetic field vector, the angle information around that vector, which is in this case one of the state of the system, is unknown, and is estimated only through the model. Because of the errors of the model, the estimation of this angle will diverge. Nevertheless, this is a special case, and most of the time, the measurement vector is not aligned with any axis of the satellite reference frame, and a more correct estimation can be obtained.

The best case during the eclipse is when the magnetic field is aligned with one diagonal of the cube, as there is some information around each axis. The results show that, after an initial error of 5 degrees, which can be obtained before the satellite enters the eclipse, the estimation does not diverge, but is less accurate than in the previous cases. The accuracy is better than 10 degrees for the angle estimation (see Figure 30 and Figure 31).

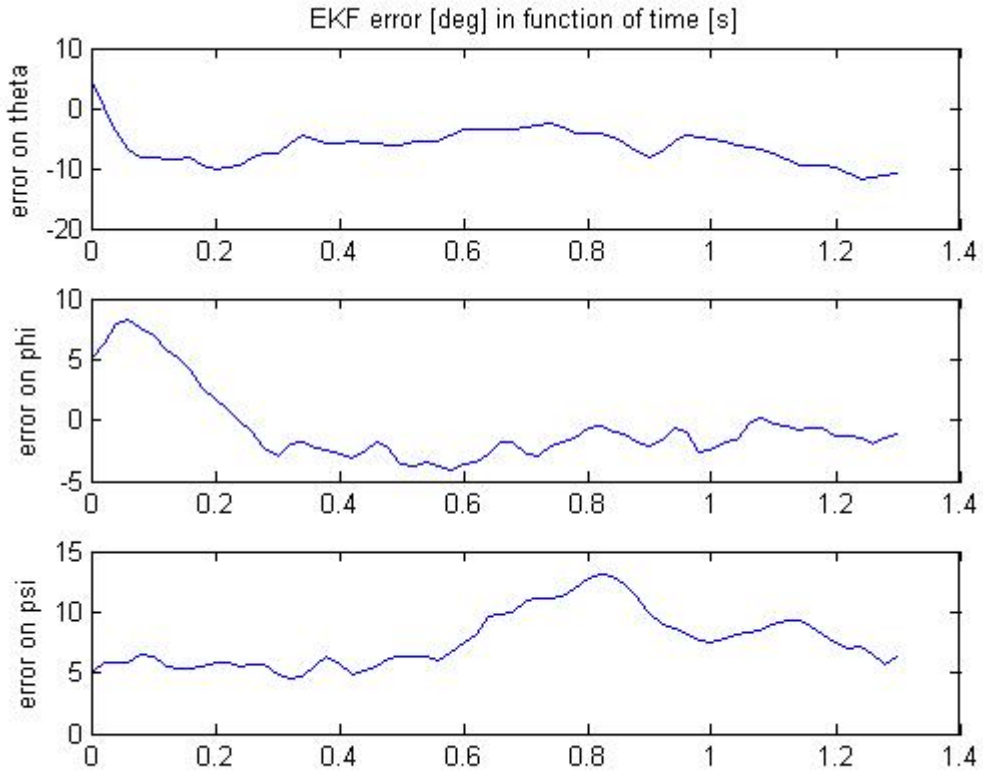

Figure 30: Error of the EKF prediction during an eclipse, when the magnetic field vector is aligned with the diagonal of the Swisscube

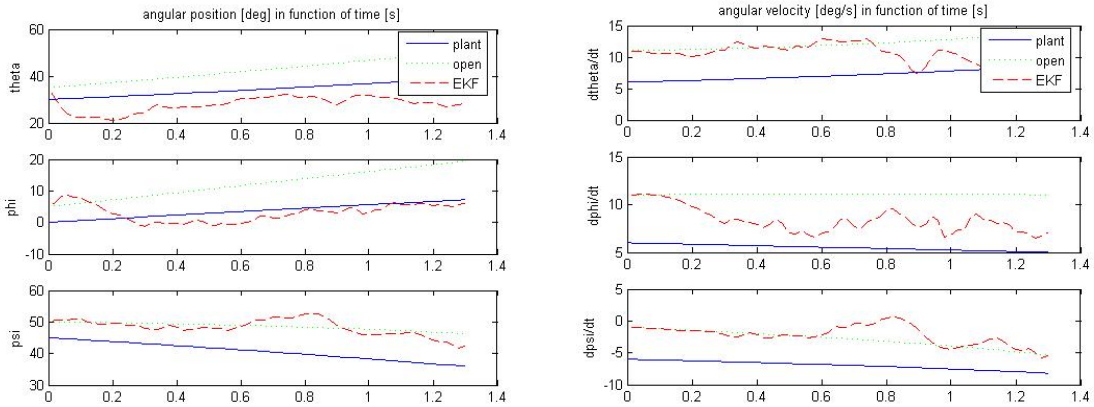

Figure 31: Angular positions and velocities, along with their estimates evolutions during an eclipse, with the magnetic field vector aligned with a diagonal of the Swisscube

As said above, the worst case is when one axis is aligned with the magnetic field. The divergence of one angle estimation can be observed, while the other two angle estimations are more accurate than in the previous case, as more information are available to these two angles (see Figure 32). We can see that the theta angle estimation follows the model (see Figure 33).

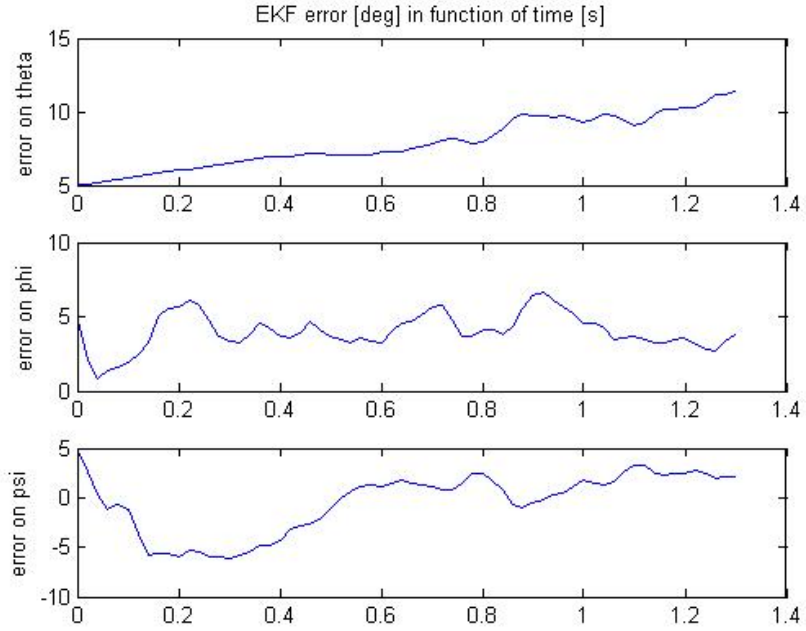

Figure 32: Evolution of the EKF error during an eclipse when the magnetic field is aligned with the first axis

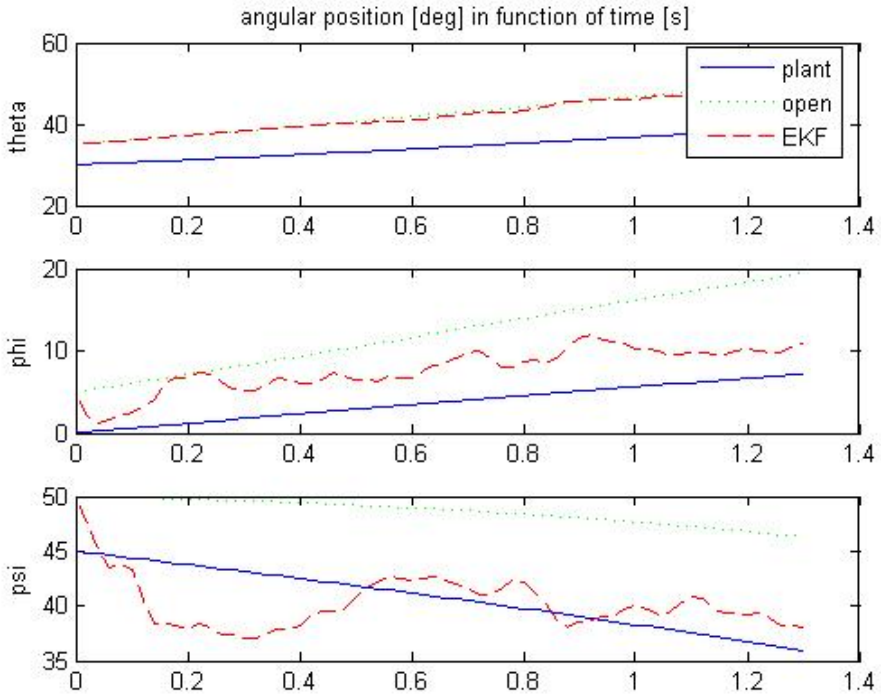

Figure 33: EKF estimates of the angular positions, compared to the open-loop estimates and real system states

What really happens during an eclipse is between these two extreme cases. It is thus probable that an accuracy below 10 degrees for every angle is not always achievable with this EKF. A better tuned version, perhaps with a quaternion model, should yield better results, but it is very unlikely that the 3-degree accuracy requirement can be reached during eclipses, even with perfect magnetometers. However, if the desired accuracy cannot be reached, the addition of a horizon sensor can solve this problem, as all three attitude angles will be measured again, as in the non-eclipse case.

5.12.2.3 Effects of the process noise

In the previous simulations, the disturbances were considered as process noise. Indeed, they are the major cause of the system not behaving exactly as expected, and it is assumed in this early work that they are not modeled. The process noise variance of the rotational speed around the i-axis is then roughly defined as $\frac{T_{disturbance}}{I_{ii}}$, ignoring the resulting gyroscopic effects for simplification purpose. Indeed, using the Newton's Law stating that $T = I\ddot{q}$ (T being the torque, I the moment of inertia and q the angular position) and the fact that the state-space model is defined by a representation of the type $\begin{bmatrix} \dot{q} \\ \ddot{q} \\ \vdots \end{bmatrix} = \begin{bmatrix} f_1 \\ f_1 \\ \vdots \end{bmatrix}$, then the torque created by the disturbance can be considered as a varying input acting on the second line of the system of equation.

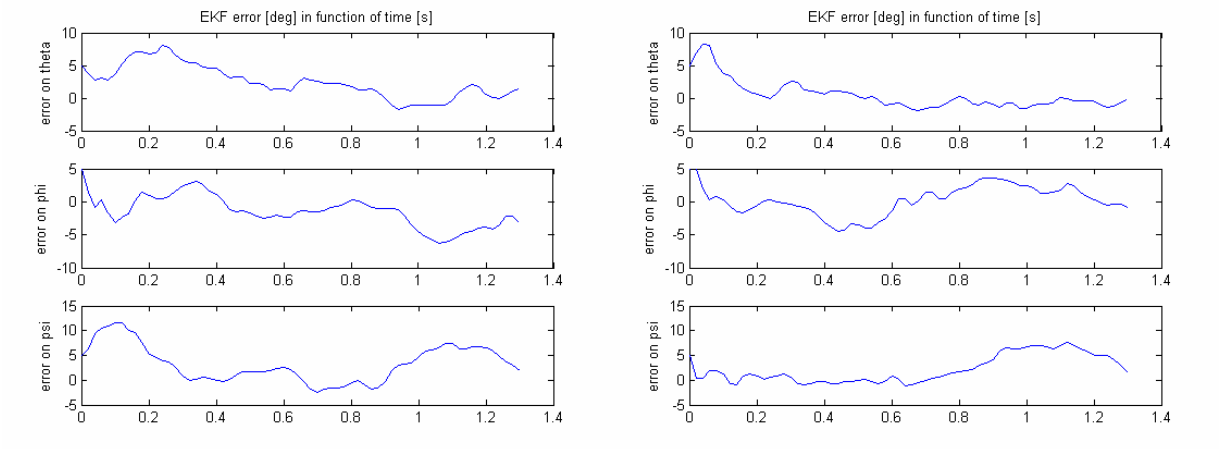

Figure 34: error of the estimation with the process noise caused by the disturbances on the left, and 10% of it on the right

In order to see the effects of the process noise, two simulations of the EKF during daytime with the same initial conditions but different process noise variances were done (Figure 34). It can be seen that when the noise is divided by ten, the estimation is significantly more accurate and stable. This shows the importance of including these disturbances in the model, as they can really decrease the determination system performances otherwise. In fact, by only adding the aerodynamic drag torque in the model, which is not very difficult given that the aerodynamic force is always applied along the velocity vector, the noise can be considered divided by ten.

5.12.2.4 Effects of the sensors accuracy

In order to perceive the advantages of having better sensors, simulations of two systems can be done (see Figure 35): one with magnetometers and solar panels, which yield an accuracy of around 5 degrees, and another one with magnetometers and an on-chip sun sensor, which yields an accuracy of 0.2 degrees. In the EKF, the measurement noise variance is considered as the accuracy of the sensors. Thus, the sensors are assumed not to be biased, and their measurements are supposed to follow a Gaussian probability distribution centered at the real value of the state.

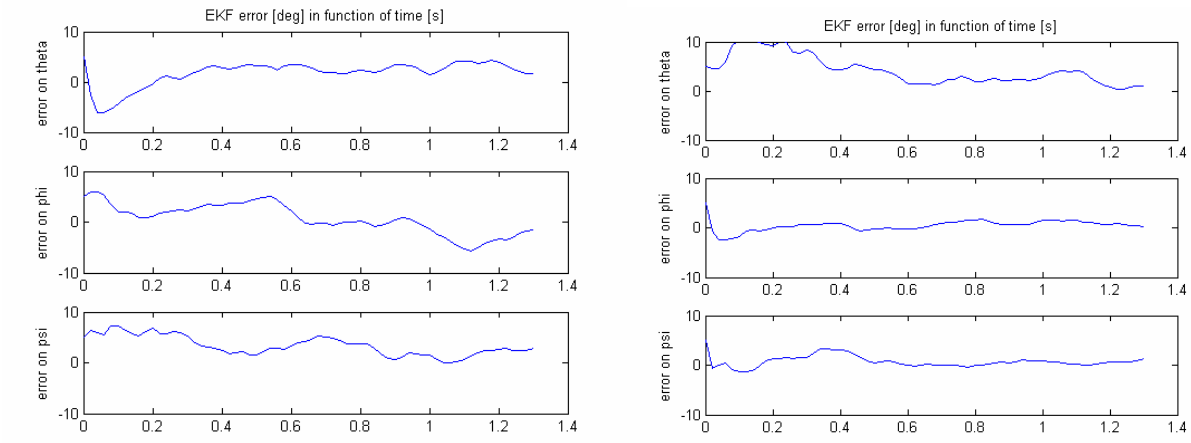

Figure 35: error of the estimation of the system with solar panels on the left, and with an on-chip sun sensor on the right

The error on angle theta is not decreased, as it was assumed in these simulations that only the magnetometers could measure this angle (or that the sun vector was parallel to this axis), but the estimation on the other angles is more stable and the convergence faster with the more accurate sensors. With an on-chip sun sensor, it is possible to have an accuracy of around 2 degrees, whereas an accuracy of slightly below 4 degrees is obtainable with the solar panels. Thus, given the low mass of the sun sensors, it is recommended to use them instead of the solar panels. The latter may provide a nearly satisfying accuracy, but this will only be the case when they yield an accuracy of 5 degrees, and their deterioration after a few months is a common phenomenon.

6 POSSIBLE TRADES

6.1 Possible Sensor Trades

The selection of sensors and actuators for the Swisscube had to be done with several aspects in mind: the power consumption, the mass, the size and the performances of each device had to be taken into account for the ACDS configuration, along with the wishes of the scientific payload group. Due to the limitations of the capabilities of the satellite, we had to loosen some otherwise unreachable requirements stated at the beginning of the project, such as the pointing accuracy of 1 degree and the scanning mode when cruising, to agree that a pointing accuracy of 3 degree and a horizon-pointing cruise mode were enough to attain our scientific goal.

With initially less than 100 g available, the mass was the most important criteria for the sensors. A star tracker would be sufficient by itself to meet the accuracy requirement, but it can hardly be implemented on a Cubesat, due to the required computation, size and mass. Here are the three possible sensor configurations, after analysis of the aforementioned parameters:

Trade 1: 3 Magnetometers and the solar panels
Trade 2: 3 Magnetometers and 1 on-chip sun sensor
Trade 3: 3 Magnetometers,1 on-chip sun sensor and a horizon sensor

6.2 Possible Actuator Trades

From the results of the in analysis in § 5.5, 5.6 and 5.7 it is possible to identify four possible actuator configurations, these are summarized in Table 16 below.

Table 16: Possible actuator configurations.

Trade 1: 3 Magnetic Torquers and 1 inertia wheel ORF x direction.
Trade 2: 3 Magnetic Torquers
Trade 3: Gravity Boom and auxiliary actuator

6.2.1 Trade 3

We note that the gravity boom trade still requires additional analysis. Using the gravity boom as passive actuator in fact we gain the control of the pointing nadir axis. However, this still leaves the rotation about the nadir axis uncontrolled. So the system still has the need to have an embarked active control system.

In addition, as described in §5.9.1, the payload axis must be pointed towards the earth this creates non-trivial problems for the fixing of the gravity gradient boom. Since the boom must point towards the nadir a mechanism has to be designed and tested to rotate the cubesat body with respect to the gravity boom in order to achieve the desired angle.

In conclusion, the exceptionally high mass of the gravity boom system, 500[g] for a 4[m] long boom, added to the added problematic for the Swisscube configuration means that this system while possible is far from an optimal solution to the Swisscube attitude control.

6.2.2 Trade 2

This trade is a possibility. While in § 5.7.2 it was seen that an inertial wheel was needed to maintain the global controllability of the system at every time instant. Recalling that this is due to the fact that the magnetic torquers have a "dead axis" parallel to the direction of the magnetic field where they cannot project a torque.

However in § 5.7.3 it was seen that recent results have proved that by taking advantage of the fact that the direction magnetic field when seen from the ORF is approximately sinusoidal then it is possible to prove the global controllability of the system. It follows that it might be possible to globally stabilize the system only with the magnetic coils.

This global controllability with only the magnetic torquers brings into play the possibility of designing a very light control systems without the need to use a wheel. If the Swisscube specifications become stringent enough to negate the possibility for an on-board inertial wheel then a magnetic torquer only control system might be considered. This trade however, might bring in to play non negligible technical complexities, in terms of control algorithms, and should be carefully studied and evaluated before adoption. Nonetheless, Trade 2 is a promising possibility which should be examined more in detail.

6.2.3 Trades 1

In terms of global simplicity Trades 1 responds best to the current needs. The total weight and power requirements are within possible system loads. The wheel magneto torquer actuator combination has been a common fixture on many different spacecraft. In addition, its provides a good controllability to the system, see §5.7.2, and the control algorithms used to control them are not excessively complex. It is in fact the preferred solution for the Swisscube actuator trade.

This trade was chosen to permit the maximum amount of inertial wheel torque control of the magnetically uncontrollable axis at the equator, where the earth's magnetic field is the weakest. This is due to the fact that at the equator the magnetic dead axis is in good approximation aligned with the ORF x axis, while in nominal condition ORF x axis is equivalent to the SRF y axis. While at the poles one can rely on a magnetic field strength approximately twice the strength than at the equator to compensate for the fact that the inertial wheels rotational axis is no longer well aligned with the magnetic field; which causes that the controllability on the "dead axis" by the wheel is reduced. However it must be noted that since the magnetic field is no longer aligned with the wheel rotational axis at the poles then in the polar region there is an excellent opportunity to perform wheel de-spinning operations.

Whether or not to use it as a Momentum wheel of Reaction wheel solution is still not defined. A decision should be made basing oneself on more accurate power requirements. At this moment both possibilities are still open. A more in depth analysis of the stability of rotations with the high gyroscopic effect due to a momentum wheel in the SRF x axis should also be performed before making a final solution.

7 BASELINE DESIGN AND ANALYSIS RECCOMENDATION

7.1 Sensors Baseline and backups

The sensors baseline is the Trade 1, with three magnetometers and the solar panels used as sun sensors, as it is a very low-mass system that require few computational resources, and it can achieve the required accuracy during daytime. Our first backup is the Trade 2, three magnetometers and an on-chip sun sensor, if possible the one from TNO presented in 5.4.1, or a custom-made photo-sensor, if a small one is unavailable from the industry, to increase the reliability of the sun sensing. Another possible alternative to this baseline concerning the sensors is the use of a horizon sensor, to be sure of the good functioning of the system during eclipses. The addition of another sensor can hardly be possible, considering the room at disposition, but it may be the only solution to achieve the required accuracy during eclipses.

7.2 Actuator Baseline and backups

The Baseline design for the actuators is Trade 1, see § 6.2.3. The three magnetic torquer and one wheel configuration gives what is the most comprehensive solution both in terms of controllability and in terms. The primary backup is trade is the possibility of using only the magnetic torquers to control the system. This solution might respond well to more stringent mass requirements. Currently Trade 3 is not considered a viable systems possibility however if the mission profile changes significantly in terms of precision it could be considered.

7.3 Future Work

7.3.1 Future work for attitude determination

Concerning the attitude determination algorithms, more advanced work can be done once a new model in quaternion is developed. For example, a deterministic algorithm can be tested, such as the q-method, and some simulation problems with the EKF will hopefully disappear, making it possible to simulate the determination system on one orbit or more. A new EKF, perhaps with new parameters being observed such as the gravity-gradient disturbance direction, could improve the estimation results during eclipses. If it is not the case, the addition of a new sensor, such as a horizon sensor, should be considered.

If a new model is not available, improvement on the current EKF simulation can be done by adding the input into the model used. One inertia wheel, or even three, can be added, but unfortunately the short time span currently available in the simulation limits the insight that this addition would give.

Further possible development includes the combination of the sensor models and of the EKF into a Simulink model. That would allow the simulation of the whole determination system, and putting it with the Simulink model with the control part would allow simulations of the total system. The

current time needed to simulate the controlled system is too big to possibly do simulations on one orbit, but once these implementation issues are solved, the achievable accuracy, consumed energy and behavior of the satellite will be known a lot more precisely.

7.3.2 Future Work Actuators and System Dynamics

There are numerous future priorities for the Control and system dynamics that must still be explored.

In § 5.9.1 and 5.9.2 it was seen that there are two aspects of the system dynamics of which further study is imperative. It is mission critical to further analyze the antenna vibration modes since their slow dynamics will probably enter in resonance at their current configuration; while the influence of the proper alignment of the inertia matrix is complex but solvable.

It is important to note that the controller presented in Section § 5.8.2 is a good start but far from a global solution. In fact the controller present is reliable only in a region and attitude close to its linearization characteristics and is unreliably with respect to constant disturbances. One possible solution to globally control the system is in fact to create a number of different controllers in different position and use the appropriate controller for the appropriate position, a gain-scheduling controller. However, there are numerous other possibilities. The strong non linearity of the system hints toward the fact that a non-linear controller might be a more effective solution. A non-linear controller might also rend feasible the possibility of using only magnetic torquers as the sole actuators. Also, in this report the actuators where dimensioned on the basis of the magnitude of the disturbances. The satisfaction of the stability requirements still need further confirmation, the verification of the system stability must be completed concurrently to the development of new algorithms. The definition of final determination of the control algorithms still requires effort.

Closely related to the control algorithms is the dynamical model. The approach used in this phase did prove adequate. However, while modeling the system with Euler angles increased its simplicity the presence of a singularity in the representation might present problems in the future. In fact it is fundamental to create a second model of the system preferably quaternion based. The new model is necessary for two reasons: to avoid singularities and to be able to validate both models by comparing their results.

Finally another important aspect that must be looked into is the definition of the hardware. Currently the wire is dimensioned in the ideal case, and an existing wire must be found or a new one fabricated in order to approach the identified characteristics. The inertial wheel motor however is the more critical aspect, in §5.5.2.3 only the dynamical requirements of the system where addressed it is necessary to find an appropriate servo that can actuate them.

7.4 Conclusions

For the sensors and attitude determination point of view, sensors were modeled and their behavior were simulated, and an estimation algorithm, the extended Kalman filter, was tested. The determination system composed of magnetometers and solar panels generate satisfying results during daytime. In this case, the accuracy of the estimation converges to below 3 degrees, even if the model is 10% wrong, as shown in the simulations. During eclipses, the estimation is less accurate, but a better EKF with a new model, or a horizon sensor can make it better. However, during past meetings of the Swisscube group, it was considered that the scientific payload team will work on making their pointing accuracy requirement less stringent. The required algorithm for the estimation is not very resource intensive, except for the linearization of the model around a point, because of

the sinus operations, but it a trade-off between computing power and memory can be done with the use of a look-up table for this kind of operations.

The sensors used are particularly effective, considering their mass, size and accuracy. Further probing of the EKF is needed in order to know if a horizon sensor is needed. The desired pointing accuracy of the Swisscube, which is more than two times more stringent than for the other studied Cubesats, might make the ACDS system require more hardware, like sensors and actuators.

For the control point of view we have identified what is a possible baseline. The current baseline has been dimensioned for the available power requirement and is within a revised global mass allocation. In fact the initial requirement for 73[g] for the system had to be revised, the current system masses 150[g], see Appendix A. This new mass however is feasible for the Cubesat system. We have in fact a base on which to start the more in depth analysis described in the previous section.

Appendix A Current Baseline mass

This is the current baseline mass created in cooperation with the systems engineer team,[Despont].

Total			**150.4**
Inertia wheel	13.5	1	13.5
Structure for wheel	7	1	7
motor	15	1	15
magnetometer	2	3	6
Magneto torquer	18.3	3	54.9
Controller	10	1	10
Latch up protection	1	1	1
Bus transceiver	2	1	2
Temperature sensor	1	1	1
Motor driver 6 transistors	1	1	1
Motor current sensor	1	1	1
Magnetometer Switch	1	1	1
Magnetotorquers current sensor	1	3	3
PCB	30	1	30
connector	4	1	4

Appendix B The Antenna Configuration [Greber]

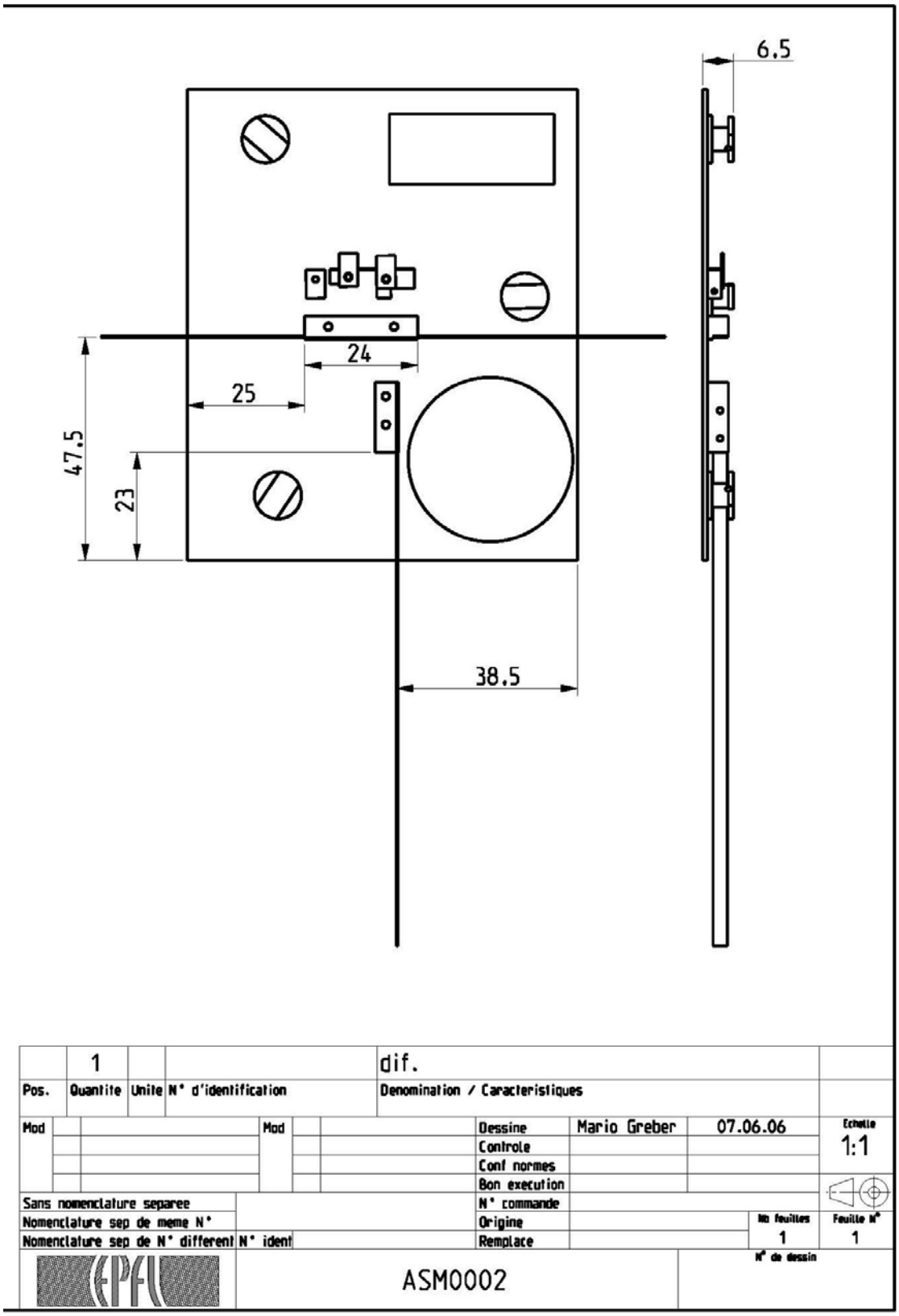

Appendix C Swisscube Inertial Properties [Roethlisberger]

C.1 Swisscube system:

Propriétés générales:

Matière: {}
Densité: 2.066E-006 (kg/(mm^3))
Volume: 4.365E+005 mm^3
Masse: 0.902 kg
Zone: 3.747E+005 mm^2

Centre de gravité:

X: -2.045 mm
Y: -2.429 mm
Z: 0.350 mm

Moments d'inertie physiques

Ixx 1.845E+003 kg mm^2
Iyx Iyy 80.337 kg mm^2 2.566E+003 kg mm^2
Izx Izy Izz -11.251 kg mm^2 -75.327 kg mm^2 2.309E+003 kg mm^2

Moments d'inertie principaux

I1: 1.836E+003 kg mm^2
I2: 2.595E+003 kg mm^2
I3: 2.288E+003 kg mm^2

Rotation XYZ/principal

Rx: 14.83 deg
Ry: -1.25 deg
Rz: 6.13 deg

C.2 Inertial wheel

NOTE Follows a different reference system:

Propriétés générales:

Matière: {}
Densité: 6.294E-007 (kg/(mm^3))
Volume: 3.004E+004 mm^3
Masse: 0.019 kg

Zone: 1.425E+004 mm^2

Centre de gravité:

X: -2.484E-015 mm

Y: 0.000E+000 mm

Z: 3.000 mm

Moments d'inertie physiques

Ixx 10.665 kg mm^2

Iyx Iyy 0.000E+000 kg mm^2 10.665 kg mm^2

Izx Izy Izz -1.972E-032 kg mm^2 3.116E-016 kg mm^2 21.216 kg mm^2

Moments d'inertie principaux

I1: 10.665 kg mm^2

I2: 10.665 kg mm^2

I3: 21.216 kg mm^2

Rotation XYZ/principal

Rx: 0.00E+000 deg

Ry: 0.00E+000 deg

Rz: 0.00E+000 deg

Distance entre COG roue inertielle et le modèle référence :

X: -47.00 mm

Y: 0 mm

Z: 0 mm

C.3 Swisscube system without inertial wheel

Propriétés générales:

Matière: {}

Densité: 2.137E-006 (kg/(mm^3))

Volume: 4.062E+005 mm^3

Masse: 0.868 kg

Zone: 3.599E+005 mm^2

Centre de gravité:

X: -0.369 mm

Y: -2.525 mm

Z: 0.389 mm

Moments d'inertie physiques

Ixx	1.823E+003 kg mm^2		
Iyx Iyy	76.665 kg mm^2	2.490E+003 kg mm^2	
Izx Izy Izz	-9.786 kg mm^2	-75.412 kg mm^2	2.233E+003 kg mm^2

Moments d'inertie principaux

I1: 1.814E+003 kg mm^2

I2: 2.519E+003 kg mm^2

I3: 2.213E+003 kg mm^2

Rotation XYZ/principal

Rx: 14.81 deg

Ry: -1.49 deg

Rz: 6.28 deg

Appendix D Swisscube configuration V14 [Roethlisberger]

Note: The complete antenna length is not shown. The single antenna in the x direction is the monopole antenna. The V shaped antenna is the dipole antenna.